Biofuel Research Journal 46 (2025) 2398-2411

Biofuel Research Journal

Journal homepage: www.biofueljournal.com

Original Research Paper

Biochar-supported highly dispersed ultrasmall Cu/ZnO nanoparticles as a highly efficient novel catalyst for CO_2 hydrogenation to methanol

Seyed Alireza Vali, Javier Moral-Vico, Xavier Font, Antoni Sánchez*

Composting Research Group (GICOM), Department of Chemical, Biological and Environmental Engineering, Universitat Autònoma de Barcelona, 08193-Bellaterra (Barcelona), Spain.

HIGHLIGHTS

- An efficient biochar-based methanol synthesis catalyst was prepared and optimized.
- Optimum loading of Cu/ZnO nanoparticles was determined to be 25 wt.%.
- Cu:Zn molar ratio was also optimized to be 2:1.
- Remarkably high STY of 496.5 $mg_{MeOH}\ g_{Cu}^{-1}\ h^{-1}$ and selectivity of 71% was obtained.
- Ultrasmall Cu/ZnO nanoparticles ranging in size around 5 nm were obtained.

GRAPHICAL ABSTRACT

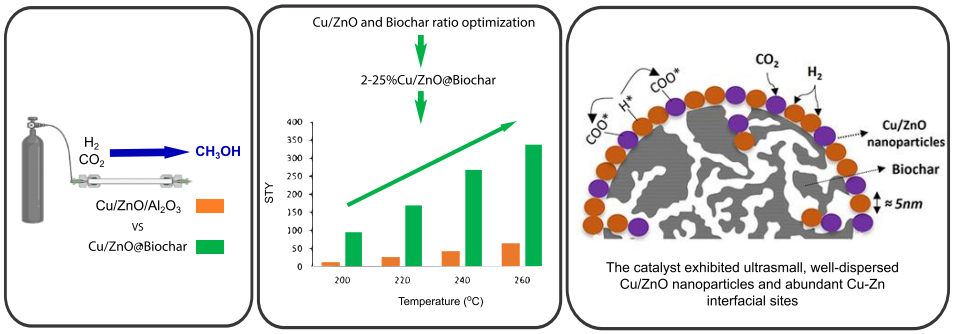

A highly efficient biochar-supported Cu/ZnO catalyst was developed for CO_2 hydrogenation to methanol, with biochar enhancing reactant adsorption and activation through its porous structure and abundant oxygen vacancies

ARTICLE INFO

Article history:
Received 27 January 2025
Received in revised form 13 April 2025
Accepted 22 April 2025
Published 1 June 2025

Keywords:
CO_2 hydrogenation
Biochar
Ultrasmall Cu/ZnO nanoparticles
Methanol synthesis
Heterogenous catalysis

ABSTRACT

Methanol synthesis via CO_2 hydrogenation is a key pathway for producing methanol. Considerable research has focused on enhancing Cu/ZnO-based catalysts for this process. In this study, biochar, a porous material derived from renewable waste, was employed to support the immobilization of Cu/ZnO nanoparticles for CO_2 hydrogenation to methanol. The catalyst developed in this work exhibited exceptional performance, with a methanol space-time yield (STY) of 496.5 $mg_{MeOH}\ g_{Cu}^{-1}\ h^{-1}$, selectivity of 71%, and stability (maintaining catalytic activity for over 45 h). These metrics significantly outperformed those of the $Cu/ZnO/Al_2O_3$ catalyst (STY of 98.6 $mg_{MeOH}\ g_{Cu}^{-1}\ h^{-1}$, selectivity of 54%, with catalytic activity loss after 25 h) under identical reaction conditions (260 °C, 1 MPa). Structural characterizations revealed that the enhanced catalytic activity and improved stability of the biochar-supported Cu/ZnO nanoparticles, relative to $Cu/ZnO/Al_2O_3$, were attributed to the enrichment of Cu-Zn interfacial sites. This was facilitated by the highly efficient dispersion and formation of ultrasmall Cu/ZnO nanoparticles on the biochar surface, along with biochar's role in enhancing H_2 and CO_2 adsorption and activation.

* Corresponding author at:
E-mail address: antoni.sanchez@uab.cat

Please cite this article as: Vali S.A., Moral-Vico J., Font X., Sánchez A. Biochar-supported highly dispersed ultrasmall Cu/ZnO nanoparticles as a highly efficient novel catalyst for CO_2 hydrogenation to methanol. Biofuel Research Journal 46 (2025) 2398-2411. DOI: 10.18331/BRJ2025.12.2.3.

Contents

Abbreviations

BC	Biochar
BET	Brunauer–Emmett–Teller
CO_2-TPD	Carbon dioxide temperature-programed desorption
EDX	Energy dispersive spectroscopy
FID	Flame ionization detector
H_2-TPD	Hydrogen temperature-programed desorption
H_2-TPR	Hydrogen temperature-programed reduction
HAADF	High-angle annular dark-field
HRTEM	High resolution Transmission electron microscopy
ICP-OES	Inductively coupled plasma optical emission spectroscopy
MOFs	Metal organic frameworks
NPs	Nanoparticles
PXRD	Powder X-ray diffraction
SEM	Scanning electron microscopy
SMSI	Strong metal-support interactions
STEM	Scanning transmission electron microscopy
STY	Space-time yield
TCD	Thermal conductivity detector
TEM	Transmission electron microscopy
TGA	Thermogravimetric analysis
XPS	X-ray photoelectron spectroscopy
XRD	X-ray diffraction
WHSV	Weight hourly space velocity

1. Introduction

The increasing release of greenhouse gases such as carbon dioxide into the atmosphere as a result of the exploitation of fossil fuels has been a major global concern in recent decades. Research has therefore focused on the capture and conversion of carbon dioxide into value-added chemicals (Markewitz et al., 2012; Du et al., 2018; Vali et al., 2018). Carbon capture and storage and chemical conversion have proven to be effective techniques for reducing carbon dioxide emissions and transitioning to renewable energy sources (Leung et al., 2014; Vali et al., 2023a and c).

In this context, the hydrogenation of carbon dioxide to methanol is of great interest, considering methanol as a potential fuel as well as a building block for the production of many industrial chemicals (Jadhav et al., 2014). However, such a reaction typically takes place under stringent conditions in terms of temperature and pressure, due to the high thermodynamic stability and low reactivity of carbon dioxide (Raudaskoski et al., 2009; Zhao et al., 2011). This has led researchers to investigate potential solid catalysts that can catalyse the methanol synthesis reaction under milder conditions. Many catalysts have been developed and studied for this purpose, with Cu-based catalysts being the most widely studied. The popularity of Cu-based catalysts is due to the competence of Cu as an active site for the hydrogenation of carbon dioxide to methanol compared to other elements (Toyir et al., 1998; Vali et al., 2023b and 2024).

Nevertheless, many studies have been carried out to date to overcome the unavoidable obstacle of Cu-based catalysts: insufficient dispersion of Cu resulting in low surface area as well as sintering and deactivation under harsh working conditions. The investigation of metal oxide supports such as CeO_2, ZrO_2, TiO_2, as well as potential porous frameworks such as zeolites and metal-organic frameworks (MOFs) to enhance Cu dispersion has been only partially successful (Lei et al., 2015; Shi et al., 2019; Si et al., 2020). However, an important issue that remains to be addressed is that due to the bulk nature of such catalysts, the majority of active sites are actually poorly accessible to the reactive gas due to lack of sufficient porosity and low specific surface area. The use of highly porous structures such as MOFs can partially solve this problem. For example, Cu and Cu/ZnO nanoparticles (NPs) encapsulated in the pores of MOFs improve the availability of active sites, and smaller NPs can be achieved due to the cavity confinement effect, thus increasing the amount of active sites (Yu et al., 2022). However, there are still concerns regarding MOF-based catalysts, including the thermostability of MOFs as well as their complex and uneconomical preparation, especially at the gram scale.

Recent advancements in CO_2 hydrogenation to methanol have focused on developing and optimizing catalysts to enhance efficiency and selectivity. Traditional Cu/ZnO-based catalysts have been extensively studied, with recent modifications involving the incorporation of alkali metals. For instance, Ding et al. (2025) demonstrated that introducing alkali metals like lithium, sodium, or potassium into CuO/ZrO_2 catalysts significantly increased methanol selectivity, achieving up to 98.9% selectivity at 8.8% CO_2 conversion. Indium oxide (In_2O_3) has emerged as a promising catalyst due to its high selectivity towards methanol. Recent studies have explored doping In_2O_3 with metals such as nickel (Ni) and cobalt (Co). Wesner et al. (2023) reported that Ni-promoted In_2O_3/ZrO_2 catalysts exhibited enhanced methanol productivity, attributed to improved hydrogen spillover and CO_2 adsorption capabilities. In another study, the development of CuO/ZnO catalyst spheres, promoted with CeO_2, ZrO_2, and CaO, has led to enhanced CO_2 conversion rates and methanol production, highlighting the importance of multi-component systems in catalytic performance (Fritsch et al., 2024). Furthermore, ternary catalysts $Pd–In_2O_3–ZrO_2$ reported by Araújo et al. (2024) have shown significant potential, leveraging synergistic effects to enhance methanol productivity and stability.

In this study, biochar was exploited as a cost-effective waste-derived material as a support for the immobilization of Cu/ZnO NPs. Biochar, as a solid carbon residue, is produced by thermochemical decomposition processes such as gasification or pyrolysis of biomass (Cha et al., 2016; Cao et al., 2017). Biomass as a natural abundant resource can be obtained from lignocellulose, crops, aquatic cultures as well as biowaste from agricultural, urban and domestic wastes and animal fats (Cha et al., 2016; Lee et al., 2017). It was hypothesized that the immobilisation of Cu/ZnO NPs on the biochar surface and within the pores could result in a better distribution of reactive sites, leading to higher methanol production. It was also suggested that biochar could facilitate the adsorption and activation of reactants, which is one of the key steps in methanol synthesis.

The biochar-supported Cu/ZnO catalyst developed in this study presents a novel and sustainable approach to CO_2 hydrogenation to methanol. Unlike

Please cite this article as: Vali S.A., Moral-Vico J., Font X., Sánchez A. Biochar-supported highly dispersed ultrasmall Cu/ZnO nanoparticles as a highly efficient novel catalyst for CO_2 hydrogenation to methanol. Biofuel Research Journal 46 (2025) 2398-2411. DOI: 10.18331/BRJ2025.12.2.3.

conventional metal oxide supports such as Al_2O_3 or ZrO_2, biochar is a renewable, low-cost material derived from biomass, aligning with green chemistry principles. Its highly porous structure enhances the dispersion of Cu/ZnO nanoparticles, preventing agglomeration and ensuring a higher density of active sites. Additionally, the functional groups present on biochar facilitate strong metal-support interactions, improving catalytic stability and reaction kinetics. Moreover, biochar's surface properties can be tuned or functionalized to optimize CO_2 adsorption and activation, further enhancing the catalyst's performance.

This novel catalyst demonstrates significant advantages in CO_2 hydrogenation, particularly in improving methanol selectivity and CO_2 conversion. Biochar's ability to modify the electronic environment of Cu/ZnO enhances CO_2 activation, leading to higher methanol yields compared to conventional supports. Its cost-effectiveness and eco-friendly nature reduce reliance on rare or expensive catalyst supports, offering a sustainable alternative for large-scale applications. Additionally, the robust structure of biochar provides enhanced thermal and mechanical stability, potentially extending the catalyst's operational lifespan. Given these benefits, biochar-supported catalysts hold promise for scalable and industrial methanol production, making the process more economically viable while promoting waste valorization.

By integrating biomass-derived materials into CO_2 hydrogenation, this study contributes to the development of efficient, cost-effective, and environmentally friendly catalysts. It bridges the gap between biomass utilization and CO_2 conversion, demonstrating that waste-derived materials can serve as high-performance catalyst supports. This work not only advances catalyst design but also aligns with global sustainability efforts, highlighting the potential of biochar as a key component in future carbon utilization strategies. Although biochar-based catalysts have been previously investigated for applications such as soil remediation, adsorption, water reclamation, biomass upgrading as well as catalysis (Cao et al., 2017; Pereira Lopes and Astruc, 2021; Alexis Parra-Orobio et al., 2023), to the best of our knowledge, there is no report on methanol synthesis and no information on Cu/ZnO NPs supported on biochar.

In this work, the main objective was to prepare a highly efficient biochar-supported catalyst and test it in carbon dioxide hydrogenation under mild conditions using a continuous laboratory-scale plug flow reactor. The catalyst was synthesized and optimized in terms of NP loading and Cu/Zn ratio. The optimal catalyst significantly exceeded the catalytic activity of the commercially used ternary $Cu/ZnO/Al_2O_3$ in terms of methanol space-time yield (STY), selectivity and stability. A detailed characterization of the catalysts was also carried out to understand the relationship between the structural properties of the catalyst and its high catalytic activity.

2. Experimental

2.1. Materials

Zinc nitrate hexahydrate ($Zn(NO_3)_2.6H_2O$), copper nitrate trihydrate ($Cu(NO_3)_2.3H_2O$), aluminium nitrate nonahydrate ($Al(NO_3)_3$, $9H_2O$) and sodium carbonate (Na_2CO_3) were purchased from Merck (Madrid, Spain). The purity of all reagents is greater than 99.0% and they were used as received. The mixture of carbon dioxide and hydrogen in a molar ratio of 1:3 was provided by Carburos Metálicos, S.A. (Barcelona, Spain). Biochar synthesised at high temperature (700ºC) was used for the experiments.

2.2. Synthesis of Cu/ZnO@BC

Prior to catalyst preparation, the biochar was sieved to obtain particles in the range of 20 to 100 microns and then thermally treated in a muffle furnace at 600°C for 3h to eliminate adsorbed water and volatile organic compounds. The synthesis of the biochar-supported catalyst samples was carried out via the co-precipitation-deposition route. The Cu/ZnO@BC (biochar is abbreviated as BC in the catalyst labels) samples with different NP loadings (20-51 wt.%) as well as different Cu/Zn molar ratios including 0.5, 1, 1.5, 2, 3, 4 were prepared and named as listed in **Table S1**. In **Table S1,** detailed amounts of all the reagents used are also given.

As an example of the synthesis of 2-25%Cu/ZnO@BC (where 2 is the Cu/Zn molar ratio and 25% is the NPs loading), 1.655 mmol (0.4 g) of $Cu(NO_3)_2.3H_2O$ and 0.827 mmol (0.246 g) of $Zn(NO_3)_2.6H_2O$ were dissolved in 200 mL of ultrapure water. Then 500 mg of biochar was added to the above solution and the mixture was left for 2 h with vigorous stirring to allow the Cu^{2+} and Zn^{2+} species to be adsorbed onto the biochar surface. A precipitant solution (Na_2CO_3, 0.025 M) was then added dropwise to the solution containing the Cu^{2+}, Zn^{2+} and biochar to induce the formation of $Cu_xZn_y(OH)_m(CO_3)_n$ crystallites on the porous structure of the biochar, while the pH of the solution was adjusted to 7.00. The solution was then transferred to a 500 mL Scharlau Minireactor HME-R/500 and allowed to age at 60 °C for 2 h to complete the formation of $Cu_xZn_y(OH)_m(CO_3)n$@BC.

Finally, the resulting slurry was washed several times with ultrapure water to remove the remaining Na^+, then centrifuged and dried at 105°C overnight to obtain the $Cu_xZn_y(OH)_m(CO_3)_n$@BC sample. CuZnO@BC particles were further obtained by calcination and reduction of $Cu_xZn_y(OH)_m(CO_3)_n$@BC. Typically, $Cu_xZn_y(OH)m(CO_3)n$@BC samples were heated in a muffle furnace at 400 °C for 3 h. Prior to catalytic tests, calcined samples were reduced with H_2 gas flow (atmospheric pressure, 3.3334×10^{-7} m^3s^{-1} at 300 °C for 2 h. Afterwards, Cu/ZnO@BC samples were ready for further characterisation and catalytic tests. 27% Cu@BC was prepared by a similar procedure. The ternary catalyst $Cu/ZnO/Al_2O_3$ (Cu/Zn/Al molar ratio: 6:3:1) was synthesised by the similar procedure, which follows the conventional commercial catalyst synthesis procedure. (Zhang et al., 2022).

2.3. Catalyst characterization

An in-depth characterization of the catalyst was performed. Scanning electron microscopy (SEM) (Merlin FE-SEM) equipped with an energy dispersive spectroscopy (EDX) detector (EDX Oxford LINCA X-Max) was employed to determine the morphology, size distribution and elemental composition of the samples. Nitrogen adsorption/desorption analyses were carried out at -196 ºC using an ASAP 2020 Micrometrics Inc (BET analyser). All samples were degassed at 80 ºC for 20 h before analysis.

Transmission electron microscopy (TEM) as well as high-angle annular dark-field scanning transmission electron microscopy (HAADF-STEM) analyses were carried out on a double-corrected transmission electron microscope (Thermo Fisher Scientific Spectra 300 (S)TEM) equipped with ultra-high energy resolution field emission gun (X-FEG) and a monochromator (Ultimono) with an acceleration voltage of 200 kV. In addition, a Super-X EDX detector was employed to perform the Energy-dispersive X-ray spectroscopy (EDX) elemental mapping. For the HRTEM and HAADF-STEM experiments, the catalyst 2-25%Cu/ZnO@BC was grinded and a part of Cu/ZnO NPs was isolated for the analysis.

The TGA analyses were performed using a thermogravimetric analyzer (TGA 7, Perkin Elmer) with a heating rate of 5ºC per min under a constant Ar flow. Crystalline structure of the catalyst samples was investigated using Powder X-ray diffraction (PXRD). The XRD patterns were recorded in a diffractometer (Panalytical X'Pert) using Cu-Kα radiation (λ=1.5418 Å). The measurements were made at room temperature at a range of 0º-80º on 2θ with a step size of 0.02º. X-ray photoelectron spectroscopy (XPS) experiments for the surface characterization were performed using a SPECS PHOIBOS150 hemispherical analyser with a monochromic X-ray source (1486.6 eV) operated at 300 W. All the measurements were carried out in an ultra-high vacuum chamber with a pressure in the $5\cdot10^{-9}$–$2\cdot10^{-8}$ torr range during data acquisition. The binding energy values were referred to that of C1s at 284.8 eV. In addition, to determine the chemical composition of catalyst samples, inductively coupled plasma optical emission spectroscopy (ICP-OES) was employed (Optima3200rl. PerkinElmer).

Furthermore, an AutoChem (Micromeritics) instrument using 12 vol% H_2/Ar at a flow of 50 N mL·min^{-1} in the temperature range of 35−800°C at a heating ramp of 10°C·min^{-1} was used for temperature-programed reduction (H_2-TPR) measurements. The amount of H_2 uptake was measured with a thermal conductivity detector. 100 mg of samples were used for each measurement. For temperature-programed reduction (H_2-TPD) experiments, the samples were first treated with He flow at 90°C, then reduced at 300 °C for 2 h in a 12 vol% H_2/Ar mixture. Then, the catalysts were cooled down to 50 °C and kept for 30 minutes, and then flushed with Ar for 1 h. Eventually, the temperature was increased linearly up to 500 °C at 5 °C/min. The outlet gases were monitored by mass spectrometry. Prior to the CO_2-TPD experiments, the catalysts were first reduced under a H_2/Ar flow (12% vol/vol, 50 mL/min) for 2 h at 300 °C, and then cooled to 35 °C. The adsorption of CO_2 was carried out at 35 °C with a feed of CO_2/He (10%

Please cite this article as: Vali S.A., Moral-Vico J., Font X., Sánchez A. Biochar-supported highly dispersed ultrasmall Cu/ZnO nanoparticles as a highly efficient novel catalyst for CO_2 hydrogenation to methanol. Biofuel Research Journal 46 (2025) 2398-2411. DOI: 10.18331/BRJ2025.12.2.3.

vol/vol) for 1 h. Then, the samples were flushed with He for 2 h and the temperature was increased under a He flow up to 800 °C at 5 °C/min.

2.4. Catalytic experiments

CO_2 hydrogenation over the catalyst samples was carried out in a fixed bed stainless steel tubular reactor (dimensions: 5.25 mm internal diameter, 89 mm length). In a typical catalytic experiment, 10 mg of catalyst was packed into the reactor using glass wool at both ends. As mentioned above, prior to the catalytic tests, the catalyst samples were calcined at 300 °C with a flow of H_2 gas. (1 MPa, 3.3334×10^{-7} m^3s^{-1}) for 2 h. Then, the temperature was cooled down and the reactant gas (H_2:CO_2=3:1) replaced the reductive gas. The standard reactions were carried out at 240 °C under 1 MPa bar with a weight hourly space velocity (WHSV) of 60000 mL $g_{cat}^{-1}h^{-1}$.

The gas samples were collected using sampling bags (SKC FlexFoil PLUS Sample Bag) and the collected methanol was analysed in a gas chromatograph (Shimadzu GC-2010, Chromeleon software) with a flame ionization detector (FID) and helium as the carrier gas. Inlet temperature was 260ºC with a flow of 50 mL/min, and the detector temperature of 280ºC. An Agilent 7890B GC System chromatograph was employed to measure CO, CO_2, and CH_4 using a thermal conductivity detector (TCD), and helium as the carrier gas with an inlet temperature of 120ºC, an inlet flow of 20 mL/min, and a detector temperature of 150ºC. The software employed was Agilent OpenLAB CDS ChemStation (Version A.01.04). Methanol STY, selectivity, and CO_2 conversion (X_{CO2}) were calculated employing **Equations 1**, **2**, and **3**, respectively:

$$CH_3OH\ STY\ \left(\frac{mg}{g_{cat}\ h}\right) = \left(\frac{Mass\ of\ methanol\ (mg)\ formed}{W_{cat}(g) \times Hour}\right) \quad \text{Eq. 1}$$

$$CH_3OH\ Selectivity\ (\%) = \left(\frac{moles\ of\ methanol\ formed}{n[CO_2]_{in} - n[CO_2]_{out}}\right) \times 100 \quad \text{Eq. 2}$$

$$X_{CO_2}(\%) = \left(\frac{n[CO_2]_{in} - n[CO_2]_{out}}{n[CO_2]_{in}}\right) \times 100 \quad \text{Eq. 3}$$

where: $n[CO_2]_{in}$ is the amount (in moles) of CO_2 at the inlet, $n[CO_2]_{out}$ stands for the amount of CO_2 at the outlet and W_{cat} is the weight of catalyst (g).

3. Results and Discussion

3.1. Synthesis and characterization of the catalysts

Prior to catalyst sample preparation, biochar was thermally treated at 600 °C for 3 h to remove moisture and unstable organic components (elemental composition and SEM images of biochar before treatment are given in **Table S2** and **Figure S1**, **Supplementary Information**). TGA decomposition patterns showed that 2.5% weight loss before 200 °C was associated with H_2O content and 48% weight loss up to 800 °C (**Fig. S2**, **Supplementary Information**), which was consistent with the weight loss of biochar measured after thermal treatment (50%).

In order to estimate the optimal amount of Cu/ZnO NPs loading on biochar, different amounts of Cu/ZnO NPs (with identical Cu:Zn molar ratio of 1:1) were prepared from 20 to 51% as shown in **Figure 1**, and the catalytic performance of the prepared samples was compared under identical conditions.

The chemical compositions were also confirmed by ICP-OES as shown in **Table S3** (**Supplementary Information**). By comparing the catalytic activities of the resulting catalysts, the optimal NPs loading was determined to be 25 wt.%, since lower methanol STY values with respect to NPs weight were obtained for the catalysts with higher than 25 wt.% Cu/ZnO content (STY values are presented in **Figure 5**, which will be further discussed in the next sections). This indicates that the additional NPs loading (above 25%) was mainly formed in bulk form as the biochar surface became saturated. Catalyst samples with different molar ratios of Cu:Zn were also prepared in order to obtain the optimum Cu:Zn ratio. The catalyst with Cu:Zn of 2:1 showed the highest methanol STY and selectivity, which was in agreement with previous studies on Cu/ZnO-based catalysts. It is reported that the reason why 2:1 is the optimal Cu:Zn ratio in the Cu/ZnO catalyst derived from the zincian-malachite ($(Cu,Zn)_2(OH)_2CO_3$) phase is that during the formation of zincian-malachite, only a maximum molar percentage of about 33% of Zn^{2+} substitution can occur in the crystal lattice of malachite ($Cu_2(OH)_2CO_3$) (Van Den Berg et al., 2016; Kattel et al., 2017b).

The scanning electron microscopy (SEM) images obtained for the catalyst sample 2-25%Cu/ZnO@BC and the as-prepared Cu/ZnO/Al_2O_3 are shown in **Figure 2a-b** and **Figure S6a-c** (**Supplementary Information**), respectively. As can be observed, for biochar supported catalysts (**Fig. 2a-b**), Cu/ZnO NPs are well dispersed on the biochar surface and no large agglomerated particles are observed, while for Cu/ZnO/Al_2O_3 (**Fig. S6a-c**, **Supplementary Information**) agglomerated lumps larger than 10 microns are highly visible.

The comparison of the BET specific surface area and pore volume values of biochar and the catalyst sample 2-25%Cu/ZnO@BC (**Table S4**) showed that Cu/ZnO NPs were also formed inside the micropores of biochar, which leads to the formation of smaller NPs due to the cavity confinement effect during synthesis and prevents NP agglomeration during the CO_2 hydrogenation reaction due to the high temperature and pressure conditions. This may be one of the factors explaining the superior stability of the biochar-based catalyst in this work compared to Cu/ZnO/Al_2O_3, which will be discussed in the next sections. The needle-like morphology of the Cu/ZnO NPs shown in **Figure 2b** is attributed to the formation of zincian malachite ($(Cu,Zn)_2(OH)_2(CO_3)$) and aurichalcite ($(Cu,Zn)_5(OH)_6(CO_3)_2$ crystalline phases in the catalyst precursor, which was confirmed by XRD (**Fig. S4**, **Supplementary Information**). It is well known that the formation of such precursor phases results in well-mixed CuO/ZnO NPs, largely due to the automatic substitution of part of the Cu by Zn during precursor ageing. (Zander et al., 2012; Kattel et al., 2017b).

The EDX elemental mapping obtained for the 2-25%Cu/ZnO@BC sample (**Fig. S3**, **Supplementary Information**) revealed the formation of well-distributed Cu/ZnO NPs on the biochar surface, which facilitated the presence of Cu and ZnO in close proximity, resulting in the formation of Cu-Zn interfaces, which are the main reactive sites for methanol synthesis from CO_2 hydrogenation. (Zander et al., 2012). In addition, the ZnO particles act as a physical spacer between the CuO particles and can prevent further agglomeration and sintering of the CuO particles, which typically occurs during catalyst preparation and during the reaction under harsh conditions. High resolution TEM analysis of Cu/ZnO NPs supported on biochar is shown in **Figure 2c-e**. The presence of intimately mixed Cu and ZnO NPs can also be clearly seen by comparing the HRTEM image (**Fig. 2e**) and STEM elemental mapping images obtained for a magnified region (denoted as area #1) (**Fig. 2f-i**). The presence of intimately mixed Cu/ZnO NPs is crucial for a synergistically highly effective Cu-ZnO system as far as methanol synthesis from CO_2 hydrogenation is concerned (Yu et al., 2022).

Due to the high degree of mixing as well as the relatively close sizes of the different Cu and ZnO crystallite systems (e.g. the d-spacing for Cu (111) and ZnO (011) were 2.31 and 2.46 Å, respectively, obtained from powder X-ray diffraction data), it is quite difficult to distinguish between Cu and ZnO crystallites. Interestingly, very small Cu and ZnO NPs (<5 nm) can be identified in the HRTEM images (**Fig. 2e**), which is equivalent to a high specific surface area of the active sites and is responsible for the excellent methanol STY obtained for the catalyst in the present study.

To study the crystalline structure of the catalyst samples, powder X-ray diffraction (PXRD) was carried out and the diffractograms are shown in **Figure 3**. The crystallographic structure of all catalyst samples was analyzed by powder X-ray diffraction as shown in **Figure 3**. The main diffraction peaks appearing in the XRD pattern of biochar at 2θ values of 20.8°, 26.6°, 36.5° and 39.4° are associated with the SiO_2 phase, while the peak appearing at 29.4° indicates the presence of the $CaCO_3$ phase. For all catalyst samples, the diffraction peaks appearing at 2θ values of 43.3°, 50.5° and 74.2° are attributed to metallic Cu indexed to (111), (002) and (022) lattice planes with a cubic crystal system (Bonura et al., 2014). In addition, hexagonal ZnO was observed at 2θ values of 31.8°, 34.3°, 36°, 47.3°, 56.8° indexed to lattice planes (010), (002), (011), (012), and (110), respectively (Palomino et al., 2018).

For the as-synthesized commercial catalyst, peaks at 66.5°(214), and 68.2° (030) appeared, which are related to formation of Al_2O_3 (Mahmoud et al., 2022). However, the diffraction peak at 35.2° indexed to the (104) lattice system of Al_2O_3 could not be clearly seen due to its overlap with the CuO

Please cite this article as: Vali S.A., Moral-Vico J., Font X., Sánchez A. Biochar-supported highly dispersed ultrasmall Cu/ZnO nanoparticles as a highly efficient novel catalyst for CO_2 hydrogenation to methanol. Biofuel Research Journal 46 (2025) 2398-2411. DOI: 10.18331/BRJ2025.12.2.3.

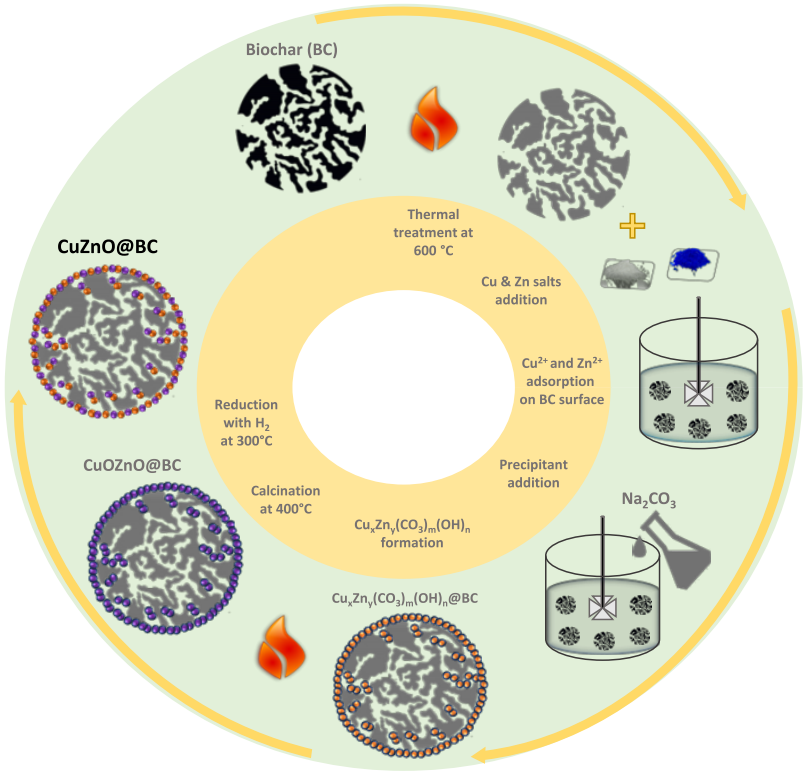

Fig. 1. Schematic procedure for the synthesis of Cu/ZnO@BC samples.

diffraction peak. Notably, both metallic Cu and CuO phases (2θ =35.6° and 38.7°) were observed for the ternary Cu/ZnO/Al_2O_3 (**Fig. 3**). This could be attributed to its incomplete reduction, as CuO was largely present in bulk form due to improper dispersion in the CuO/ZnO/Al_2O_3 catalyst. However, no diffraction peaks corresponding to CuO were identified in the Cu/ZnO@BC samples. This confirms the initial hypothesis of improved dispersion of Cu active sites on the biochar surface.

In addition, enlarged XRD patterns for the 27%Cu@BC, 2-25%Cu/ZnO@BC and Cu/ZnO/Al_2O_3 catalysts are shown in **Figure 2d-g**. It can be seen that the peaks corresponding to metallic Cu (2θ=43.3°, 50.4°) are slightly shifted to lower diffraction angles for the catalyst 2-25%Cu/ZnO@BC (2θ=43.23°, 50.15°) compared to the identical Cu peaks for the catalysts 27%Cu@BC (2θ=43.36°, 50.4°) and Cu/ZnO/Al_2O_3 (2θ=43.36°, 50.5°). Knowing that the diffraction peaks of the CuZn alloy ($Cu_{0.7}Zn_{0.3}$) are positioned at 2θ=42.4° and 49.5° (Zhang et al., 2022), the shift in the Cu diffraction peaks is probably due to the partial reduction of ZnO at the Cu-ZnO interface leading to the formation of a fractional Cu-Zn alloy. This suggests that the proper dispersion of CuO/ZnO NPs on biochar has facilitated their reduction. The reduction of ZnO may occur to some extent at the Cu-ZnO interface due to hydrogen spillover from Cu (Fichtl et al., 2014; Kattel et al., 2017b).

XPS measurements were carried out to study the electronic surface structure of catalyst samples. In the Cu 2p XPS spectra, the peaks at 952.7 and 932.8 eV corresponded to $2p_{1/2}$ and $2p_{3/2}$ of Cu/Cu^+ species, respectively (**Fig. 4a**) (Yu et al., 2021a; Mitsuka et al., 2021; Xin et al., 2021). The peaks at binding energies of 954.9 and 934.8 eV as well as the satellite peaks (denoted as sat in the **Fig. 4a**) indicated the presence of Cu^{2+} species. As can be observed, the relative Cu^{2+} fraction in the catalyst Cu/ZnO/Al_2O_3 (19.1%) is considerably higher in comparison to that for the sample 2-25%Cu/ZnO@BC (7.3%), which could be due to deficient reduction of Cu/ZnO/Al_2O_3 as was seen before also in XRD patters. However, a small fraction of Cu^{2+} in XPS spectrum of Cu 2p for 2-25%Cu/ZnO@BC contradicts the XRD results as there were no peaks corresponding to CuO in XRD pattern of 2-25%Cu/ZnO@BC sample. This occurs because surface Cu can be easily oxidized in air and XPS analysis is surface-sensitive.

Furthermore, the XPS spectra for Zn 2p are displayed in **Figure 4b**, as well. The peaks with binding energies of 1021.7 and 1044.8 eV were identified as Zn $2p_{3/2}$ and Zn $2p_{3/2}$, respectively, which are ascribed to the lattice zinc in zinc oxide (Jain et al., 2020). The O1s spectra for the catalyst samples are also demonstrated in **Figure S5a**. The peaks at 529.8 and 530.1 eV are associated with the lattice oxygen for the samples 2-25%Cu/ZnO@BC and Cu/ZnO/Al_2O_3, respectively. The characteristic peaks for surface hydroxy group (-OH) also appeared at binding energy of 532.9 eV. In addition, the binding energy of 531.4 eV was attributed to oxygen deficient region or oxygen vacancies within the ZnO matrix (Yu et al., 2021b). The oxygen vacancies seem to be more abundant in the catalyst 2-25%Cu/ZnO@BC compared to the as-prepared Cu/ZnO/Al_2O_3. Higher methanol STY values given by catalyst 2-25%Cu/ZnO@BC compared to Cu/ZnO/Al_2O_3 is likely to be also attributed to such oxygen vacancy richness in biochar-supported catalyst. It is well known that the presence of such oxygen vacancies in the support can contribute to the CO_2 adsorption and activation via charge transfer mechanism (Barlocco et al., 2023).

Moreover, the Auger Zn $L_3M_{4.5}M_{4.5}$ can serve as a sensitive indicative of oxidation status of Zn. The Auger region consists of two peaks at around 495 and 498 eV, corresponding to Zn(0) and Zn(II), respectively (**Fig. S5b**, **Supplementary Information**). The presence of Zn(0) can be either attributed to rich oxygen vacancies in the very small ZnO NPs or be a result of partial alloying of Zn into metallic Cu NPs (Ullah Awan et al., 2012). As is shown in **Figure S5** (**Supplementary Information**), the catalyst 2-25%Cu/ZnO@BC demonstrated higher Zn(0) presence than Cu/ZnO/Al_2O_3. This is due to the higher degree of Cu and Zn mixing and their excellent dispersion while supported on biochar, which results in the formation of small NPs as well as facile partial reduction of Zn during the reduction using the spillover of H_2 from Cu NPs. Finally, as shown in **Figure S6** (**Supplementary Information**), the XPS spectrum of Al 2p was partially overlapped with Cu 3p for the commercial catalyst Cu/ZnO/Al_2O_3. The peak at 74.2 eV corresponded to Al-O-Al bond (Song et al., 2022).

Please cite this article as: Vali S.A., Moral-Vico J., Font X., Sánchez A. Biochar-supported highly dispersed ultrasmall Cu/ZnO nanoparticles as a highly efficient novel catalyst for CO_2 hydrogenation to methanol. Biofuel Research Journal 46 (2025) 2398-2411. DOI: 10.18331/BRJ2025.12.2.3.

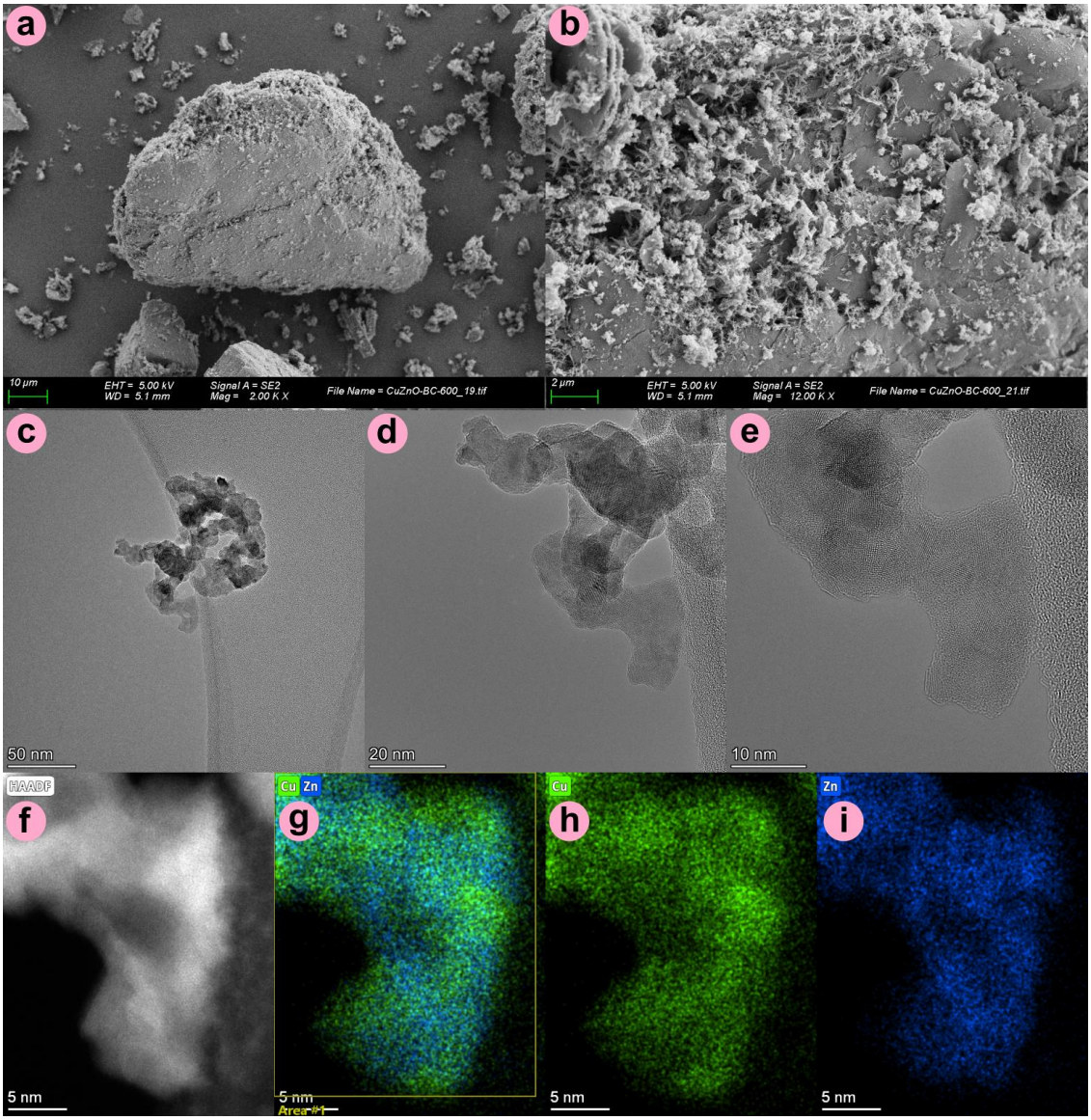

Fig. 2. (a-b) Scanning electron microscopy images; **(c-e)** High-resolution transmission microscopy images; **(f-i)** High-angle annular dark field and Scanning transmission electron microscopy coupled with energy dispersive spectroscopy elemental mapping images of 2-25%Cu/ZnO@BC sample.

3.2. Catalytic performance of catalyst samples

To evaluate the performance of the catalysts, the hydrogenation reaction of carbon dioxide to methanol was carried out under continuous conditions using several catalyst samples. First, biochar-supported Cu/ZnO samples with different NP loading (Cu:Zn molar ratio of 1) were tested at 240°C and 1 MPa. Methanol STY (with respect to Cu/ZnO NPs weight) and selectivity values are presented in **Figure 5a** to determine the best NPs loading. As can be seen in **Figure 5a**, the methanol STY of 222.7 $mg_{MeOH}\ g_{NPs}^{-1}\ h^{-1}$ was obtained for the catalyst sample with 25 wt.% Cu/ZnO NPs, which was the highest among the samples with different NPs loadings. Therefore, 25% was found to be the most efficient NPs loading on biochar.

The lower STY value for the sample with 20% w/w Cu/ZnO can be attributed to the lack of sufficient NPs to saturate the biochar surface, while the gradual decrease in STY values with increasing NP loading above 25% can be attributed to the presence of additional NPs (above 25%) in bulk form due to the lack of sufficient biochar surface to accommodate the remaining NPs (**Fig. 5a**). More NPs present in bulk form equates to less available Cu/ZnO active sites, resulting in lower methanol production. In addition, the methanol selectivity values also underwent a gradual decrease with the increase of Cu/ZnO in bulk form, which can be attributed to the dominance of the reverse water gas shift reaction (RWGS) over the poorly dispersed and partially phase separated CuO NPs (Yu et al., 2022) in the samples with relatively high Cu/ZnO contents.

Furthermore, the catalyst sample with 25% Cu/ZnO content was optimised in terms of Cu:Zn molar ratio. As shown in **Figure 4b**, the catalyst sample (2-25%Cu/ZnO@BC) with Cu:Zn molar ratio of 2:1 gave the highest methanol STY (271.6 $mg_{MeOH}\ g_{NPs}^{-1}\ h^{-1}$) and selectivity (81.8%) at 240 °C and 1 MPa. In addition, as shown in **Figure 5c-d** and **Figure S7**, both methanol STY and CO_2 conversion increased with increasing reaction temperature, which is expected for the methanol synthesis reaction (Kattel et al., 2017a). **Figure S7** (**Supplementary Information**) shows that the increase in WHSV induces an increase in methanol STY, while the CO_2 conversion decreases with the increase in WHSV, which is attributed to the insufficient contact time between the reaction gas and the catalyst (Xin et al., 2023).

Please cite this article as: Vali S.A., Moral-Vico J., Font X., Sánchez A. Biochar-supported highly dispersed ultrasmall Cu/ZnO nanoparticles as a highly efficient novel catalyst for CO_2 hydrogenation to methanol. Biofuel Research Journal 46 (2025) 2398-2411. DOI: 10.18331/BRJ2025.12.2.3.

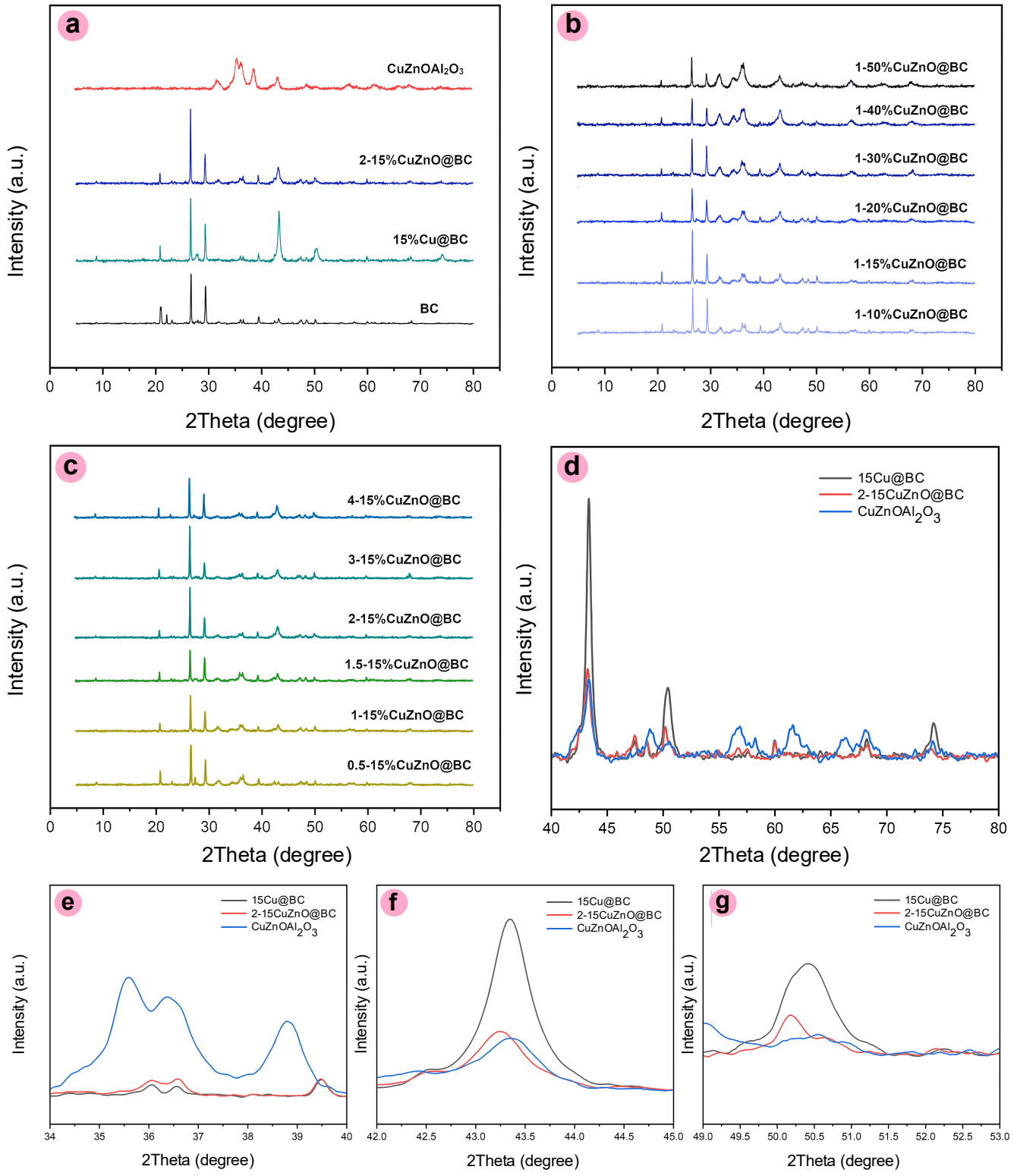

Fig. 3. X-ray diffraction patterns of **(a-c)** all the catalyst samples, **(d-g)** 27%Cu/ZnO@BC, 2-25%Cu/ZnO@BC, and Cu/ZnO/Al_2O_3 in lower 2theta ranges.

The catalytic performance of the best catalyst 2-25%Cu/ZnO@BC was then compared with the as-prepared commercial Cu/ZnO/Al_2O_3 at different reaction temperatures (Fig. 4d). The catalyst 2-25%Cu/ZnO@BC showed a manifold methanol STY as well as a slightly improved selectivity compared to the ternary Cu/ZnO/Al_2O_3 at all reaction temperatures (reaction pressures for all tests were 10 bar). As an example, for the reaction conditions of

Please cite this article as: Vali S.A., Moral-Vico J., Font X., Sánchez A. Biochar-supported highly dispersed ultrasmall Cu/ZnO nanoparticles as a highly efficient novel catalyst for CO_2 hydrogenation to methanol. Biofuel Research Journal 46 (2025) 2398-2411. DOI: 10.18331/BRJ2025.12.2.3.

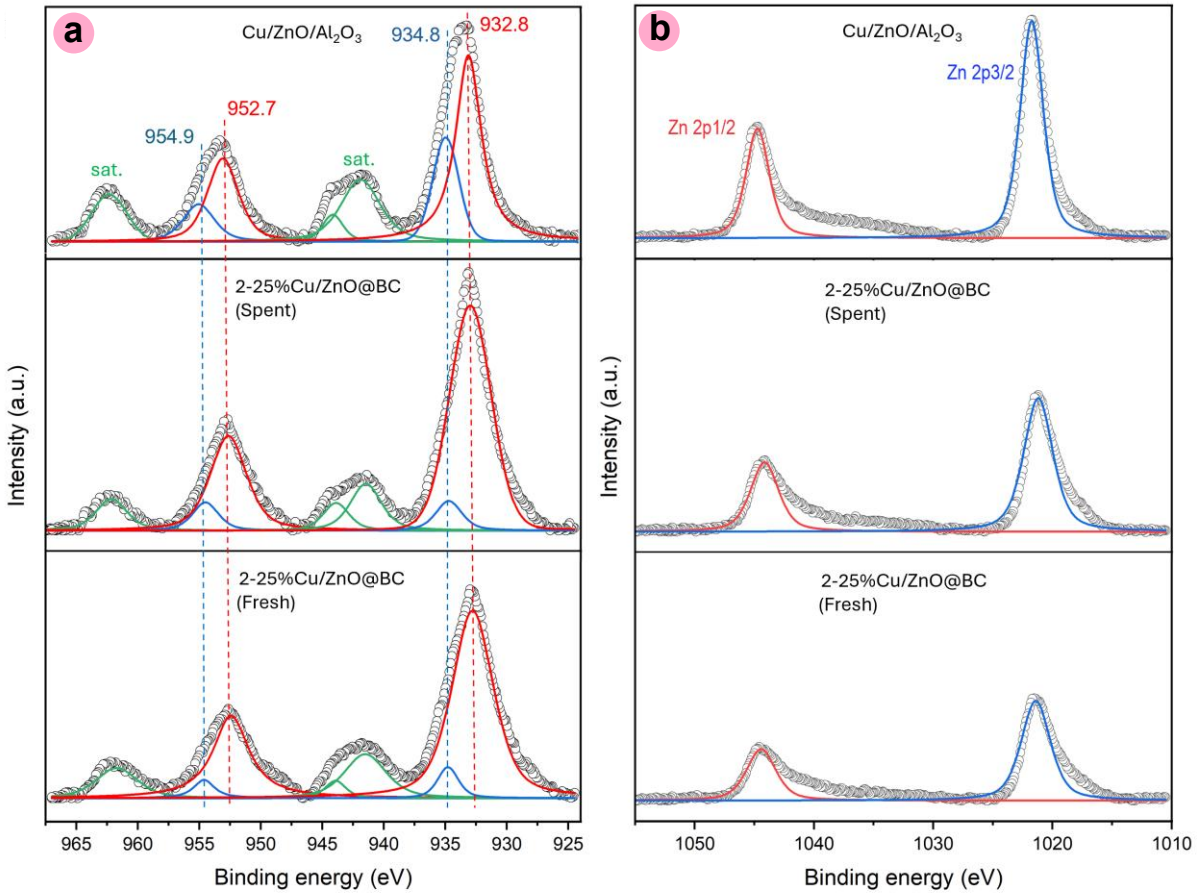

Fig. 4. (a) Cu 2p and **(b)** Zn 2p XPS spectra of 2-25%Cu/ZnO@BC (fresh), 2-25%Cu/ZnO@BC (spent), and Cu/ZnO/Al_2O_3 samples.

260 °C and 1 MPa bar, the methanol STY of the 2-25%Cu/ZnO@BC catalyst was 341.2 $mg_{MeOH}\ g_{NPs}^{-1}\ h^{-1}$ (496.5 $mg_{MeOH}\ g_{Cu}^{-1}\ h^{-1}$), which was about 5.2 times higher than the STY of 65.73 $mg_{MeOH}\ g_{NPs}^{-1}\ h^{-1}$ obtained for as-prepared ternary Cu/ZnO/Al_2O_3 (98.6 $mg_{MeOH}\ g_{Cu}^{-1}\ h^{-1}$). Such an improvement in methanol STY and selectivity highlights the significant effect of proper dispersion of NPs on their catalytic activity. Therefore, it can be concluded that by supporting Cu/ZnO NPs on the biochar surface, a significantly larger amount of active sites are accessible to the reactant gases compared to the CuZnOAl_2O_3 catalyst.

The methanol selectivity values obtained for the 2-25%Cu/ZnO@BC catalyst (71%) were relatively higher than those of the ternary Cu/ZnO/Al_2O_3 (54%) (**Fig. 4e**). The higher methanol STY and selectivity values for the 25%Cu/ZnO@BC catalyst compared to Cu/ZnO/Al_2O_3 could be attributed to the following, as mentioned above. First, the dominance of the RWGS reaction over the bulk phase separated CuO NPs, which are more abundant in Cu/ZnO/Al_2O_3 due to improper dispersion. Second, the relatively superior methanol selectivity for the biochar-supported catalyst could be due to the abundance of Cu-Zn interfacial sites as a result of the more efficient alloying of Zn with the Cu surface in the case of the biochar-supported Cu/ZnO catalyst (Wang, 2017).

In addition, the higher concentration of oxygen vacancies in the biochar-supported catalyst and their contribution to CO_2 adsorption and activation may also account for the higher catalytic performance demonstrated by the biochar-supported catalyst introduced in this work. Furthermore, with the increase of the reaction temperature from 200 to 260 °C, the methanol STY increased from 99 to 341.2 $mg_{MeOH}\ g_{NPs}^{-1}\ h^{-1}$, while the selectivity decreased from 100 to 71%, which is due to the endothermic nature of the RWGS reaction and its dominance at higher temperatures compared to the exothermic methanol synthesis reaction (Gaikwad et al., 2016). The activation energy (Ea) for CO_2 hydrogenation to methanol over 2-25%Cu/ZnO@BC was then calculated to be 46.13 $kJ{\cdot}mol^{-1}$ from Arrhenius plot (**Fig. S8**, **Supplementary Information**).

Finally, the stability of 2-25%Cu/ZnO@BC and Cu/ZnO/Al_2O_3 was investigated and compared as shown in **Figure 5e-f** (240°C, 10bar, WHSV of 12000 mL $g_{cat}^{-1}\ h^{-1}$). Both 2-25%Cu/ZnO@BC and Cu/ZnO/Al_2O_3 retained more than 95% of their catalytic activity after 44 h of catalytic reaction. Interestingly, the methanol selectivity of the 2-25%Cu/ZnO@BC catalyst was maintained after 44 h of operation, while that of the ternary Cu/ZnO/Al_2O_3 gradually decreased after 20 h of reaction. The lack of stability for ternary Cu/ZnO/Al_2O_3 has been reported in many similar studies and is attributed to sintering of Cu NPs due to harsh reaction conditions, resulting in phase separation of Cu and ZnO (Yang et al., 2021).

It is believed that a higher degree of dispersion of NPs on biochar resulted in facilitated migration of ZnO species to the Cu phase. It is known that Cu-Zn strong metal support interactions (SMSI), as well as ZnO species acting as physical spacers between Cu NPs, prevent further Cu agglomeration and Cu-Zn phase separation (An et al., 2017). These results are consistent with the higher levels of Cu-Zn alloying demonstrated by XRD and XPS studies. Finally, in order to evaluate the catalytic performance of the biochar-supported catalyst with respect to other studies, a detailed comparison with literature values was performed (**Table 1**). As can be seen in **Table 1**, the catalyst developed in this study shows superior catalytic performance compared to the majority of catalysts previously used in other studies.

3.3. Mechanism study of CO_2 hydrogenation over catalysts

Firstly, H_2-TPR was carried out to compare the reduction behaviour of the catalyst samples (**Fig. 6a**). A comparison between the H_2-TPR profiles

Please cite this article as: Vali S.A., Moral-Vico J., Font X., Sánchez A. Biochar-supported highly dispersed ultrasmall Cu/ZnO nanoparticles as a highly efficient novel catalyst for CO_2 hydrogenation to methanol. Biofuel Research Journal 46 (2025) 2398-2411. DOI: 10.18331/BRJ2025.12.2.3.

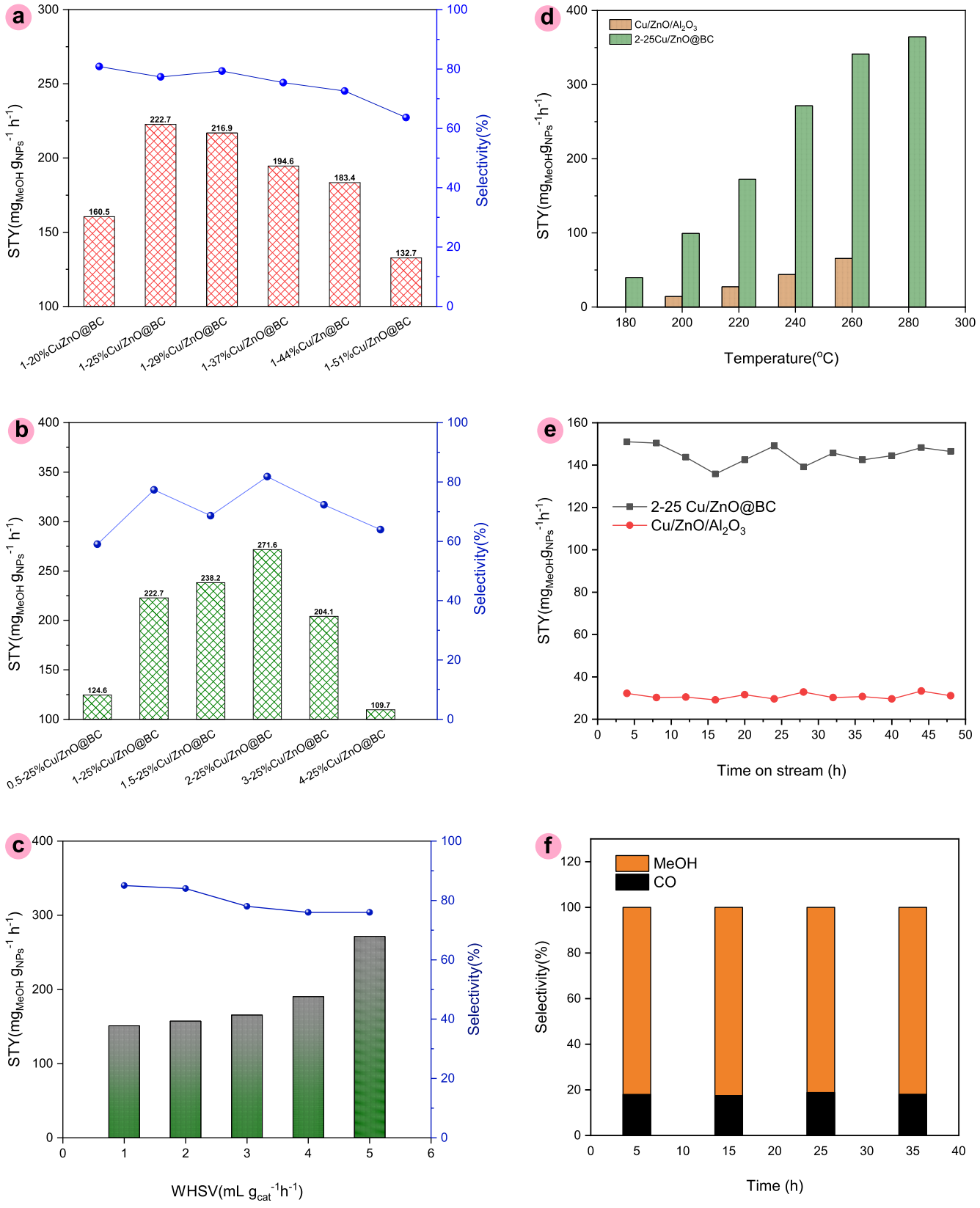

Fig. 5. Catalytic performace of the catalyst samples at reaction conditions 240°C and 1 MPa, and WHSV=60000mL $g_{cat}^{-1}h^{-1}$ for : **(a)** biochar supported Cu/ZnO catalysts with different Cu/ZnO contents; **(b)** 25%Cu/ZnO@BC catalyst with different Cu:Zn ratios; **(c)** 2-25%Cu/ZnO@BC catalyst at different work hourly space velocity (WHSV) values; **(d)** 2-25%Cu/ZnO@BC and Cu/ZnO/Al_2O_3 catalysts at different temperatures; **(e-f)** stability results of 2-25%Cu/ZnO@BC and Cu/ZnO/Al_2O_3 catalysts (WHSV=12000 mL $g_{cat}^{-1}h^{-1}$).

Please cite this article as: Vali S.A., Moral-Vico J., Font X., Sánchez A. Biochar-supported highly dispersed ultrasmall Cu/ZnO nanoparticles as a highly efficient novel catalyst for CO_2 hydrogenation to methanol. Biofuel Research Journal 46 (2025) 2398-2411. DOI: 10.18331/BRJ2025.12.2.3.

Table 1.
Catalytic performance comparison of different Cu-based methanol synthesis catalysts.

Catalyst	T[a] (°C)	P[b] (bar)	Methanol STY ($mg_{MeOH}\ g_{cat}^{-1}h^{-1}$)	Methanol Selectivity (%)	Ref.
CuO-ZnO-ZrO2-Al_2O_3	240	20	262.7	74.2	Fan and Wu (2016)
CuO-ZnO-ZrO_2-Al_2O_3/rGO	240	20	310.7	78.9	Fan and Wu (2016)
Cu/ZnO/ZrO_2	270	50	213.0	56.8	Phongamwong et al. (2017)
TiO_2/CuO-ZnO-Al_2O_3	260	26	97.7	30.98	Zhang et al. (2011)
CuO/ZnO/Al_2O_3@chitosan	260	10	92.44	90	Vali et al. (2023b)
15%-Cu/Nb_2O_5 aerogel	250	30	18.15	92.3	Xin et al. (2023)
Cu_1/ZrO_2single-atom catalyst	180	3	6.4	100	Zhao et al. (2022)
2-25%Cu/ZnO@BC	260	10	341.2	71	**Present Study**

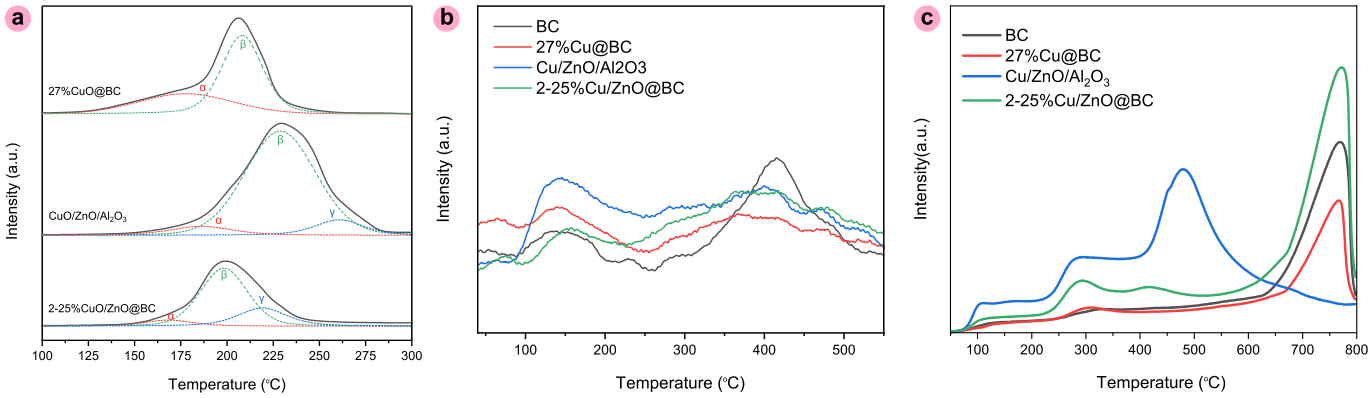

Fig. 6. (a) Hydrogen temperature-programmed reduction (H_2-TPR); **(b)** Hydrogen temperature-programmed desorption (H_2-TPD); **(c)** Carbon dioxide temperature-programmed desorption (CO_2-TPD) profiles for catalyst samples.

for three catalysts 27%CuO@BC, 2-25%CuO/ZnO@BC and CuO/ZnO/Al_2O_3 is made to understand the effect of biochar as a support on the reducibility of the catalysts. The peaks at 125-290 °C are attributed to different types of CuO species with different sizes or interactions with the supports. The first two reduction peaks (α and β) appearing at lower temperatures correspond to highly dispersed CuO species interacting moderately and strongly with supports.

In general, the reduction peaks for 27%CuO@BC and 2-25%CuO/ZnO@BC catalysts are significantly shifted to lower temperatures compared to CuO/ZnO/Al_2O_3 sample, highlighting the remarkable effect of biochar support on the dispersion of CuO NPs. Moreover, α and β peaks for 2-25%CuO/ZnO@BC catalyst appeared at lower temperatures compared to 27%CuO@BC, indicating the influence of SMSI between CuO and ZnO on the reducibility of CuO species.

In addition, the reduction temperature of CuO species gradually increases with increasing NPs content in biochar-supported catalysts (**Fig. S9**), which can be explained by the higher proportion of agglomerated CuO species present in catalyst samples with higher NPs loading, indicating the gradual saturation of the biochar surface to accommodate NPs. Nevertheless, as can be seen in **Figure S9** (**Supplementary Information**), the CuO species in all biochar-supported samples were reduced at lower temperatures than those in the ternary CuO/ZnO/Al_2O_3, indicating the highly improved dispersion of NPs in all biochar-supported catalysts compared to CuO/ZnO/Al_2O_3.

In order to study the adsorption and activation of H_2 on the catalysts, H_2-TPD experiments were carried out and the patterns are shown in **Figure 6b**. The desorption peaks at lower temperatures (100-200 °C) correspond either to the desorption of atomic hydrogen on surface-dispersed Cu sites or to generally weakly chemisorbed H_2 on the samples, while the peaks located at higher temperatures (300-500 °C) are attributed to strongly adsorbed hydrogen species, possibly due to chemisorption on metal oxide sites or on defects and stronger binding sites, which require higher energy (temperature) to desorb (Liao et al., 2017). However, these are less likely to be due to Cu-Zn interfaces and more likely to be related to individual oxide phases or SMSI (Huang et al., 2015; Liao et al., 2017). The intermediate peaks in the 200-300 °C range typically correspond to Cu-Zn interfacial sites generated as a result of SMSI, which regulates the binding energy of adsorbed hydrogen on Cu sites (Behrens et al., 2012). First, as a carbon-based material, biochar typically has a variety of weak adsorption sites for hydrogen. The broad peak suggests that hydrogen is weakly bound to its surface, probably due to physisorption on porous structures or functional groups available on the surface of biochar. This behaviour suggests that biochar alone does not have strong adsorption sites for hydrogen.

Comparing the intensity of the intermediate peaks in the 2-25%Cu/ZnO@BC and Cu/ZnO/Al_2O_3 samples, it is obvious that the intensity of such peaks is slightly higher in the Cu/ZnO/Al_2O_3 sample. However, when normalised to the amount of active material and considering that the 2-25%Cu/ZnO@BC catalyst has less than 30 wt.% Cu/ZnO compared to Cu/ZnO/Al_2O_3, it can easily be concluded that the 2-25%Cu/ZnO@BC catalyst shows a remarkably efficient use of its Cu-Zn sites for hydrogen adsorption. The relatively strong peak despite the lower loading indicates a high degree of dispersion and effective utilisation of the Cu-Zn interfacial sites on the biochar support. This is consistent with the higher degree of alloying observed for 2-25%Cu/ZnO@BC as a result of the strong metal-support interaction. It can therefore be concluded that although biochar itself does not provide sites for effective hydrogen adsorption for methanol synthesis, it indirectly affects hydrogen adsorption and activation by enhancing Cu-Zn dispersion and alloying.

In addition, the H_2-TPD patterns for the BC-supported catalysts with higher NP content, presented in **Figure S10b** (**Supplementary**

Please cite this article as: Vali S.A., Moral-Vico J., Font X., Sánchez A. Biochar-supported highly dispersed ultrasmall Cu/ZnO nanoparticles as a highly efficient novel catalyst for CO_2 hydrogenation to methanol. Biofuel Research Journal 46 (2025) 2398-2411. DOI: 10.18331/BRJ2025.12.2.3.

Information), show relatively higher H_2 uptake at both low and high temperature ranges due to the presence of higher Cu contents, especially in bulk form. This is consistent with a gradual increase in the STY values calculated with respect to the total catalyst weight ($mg_{MeOH}\ g_{cat}^{-1}\ h^{-1}$) as shown in **Figure S10a**. Furthermore, in this figure it can be seen that the intensity of the intermediate peaks decreases for the samples with more than 37 wt.% Cu/ZnO (green and purple) as well as for the samples with less than 25 wt.% Cu/ZnO (black), indicating the optimum weight percentage of Cu/ZnO in terms of the highest intensity of the intermediate peaks corresponding to Cu-Zn interfacial sites. This corresponds to the highest STY value with respect to the weight of NPs ($mg_{MeOH}\ g_{NPs}^{-1}\ h^{-1}$) obtained for the sample with 25 wt.% Cu/ZnO, as shown in **Figure 5a**.

CO_2-TPD experiments were carried out on the catalyst samples to investigate the adsorption and activation of CO_2 on the catalysts and the results are shown in **Figure 6c**. All catalyst samples contain peaks at low temperature (50-200 °C), intermediate temperature (200-450 °C) and higher temperatures associated with weak, intermediate and strong basic sites respectively (Shi et al., 2019; Li et al., 2023). Peaks at lower temperatures are associated with linear adsorption forms, while peaks at intermediate and higher temperatures are associated with bridge-bonded and horizontal adsorption forms. Linear adsorptive forms are attributed to single adsorption sites and exhibit weak adsorption, whereas bridge-bonded and horizontal adsorptive forms are associated with double adsorption sites and exhibit stronger adsorption (Olsbye et al., 2020; Stawowy et al., 2020; Chen et al., 2023).

As can be seen in **Figure 6c**, biochar (black curve) shows a strong peak at high temperatures (700-800 °C) associated with very strong basic sites for CO_2 adsorption and activation. At identical positions, both biochar supported catalysts show identical peaks with different intensities. Interestingly, the 2-25%Cu/ZnO@BC catalyst presents the peak with the highest intensity (indicating the most abundant strong basic sites) compared to the biochar and 27%Cu@BC samples. Such abundant strong basic sites in catalyst 25%Cu/ZnO@BC can be attributed to interfacial Cu-ZnO-biochar sites generated at the interface of Cu, ZnO and biochar (Gutterød et al., 2020; Yang and Jiang, 2020). This is evidenced by the appearance of another peak at moderate temperatures (around 425 °C), which was only observed for the 25%Cu/ZnO@BC catalyst. These results explain the promising methanol STY values as well as the improved selectivity and stability performance of the 25%Cu/ZnO@BC catalyst developed in this study.

4. Preliminary cost analysis

To assess the economic feasibility of the biochar-supported catalyst introduced in this study in comparison to the commercial catalyst for industrial applications, a comprehensive cost analysis was conducted. This analysis considered both the material costs and the energy consumption associated with the catalyst preparation process. The cost estimates for the raw materials and energy usage were derived from a combination of general market prices, literature values, and typical industry cost ranges. It is important to note that these estimates serve as a reasonable cost range; however, local pricing, supplier-specific quotes, and variations in manufacturing conditions could influence the final costs. For more precise estimates, direct consultation with suppliers or cost assessments based on local conditions would be necessary.

Based on the material and energy cost data presented in **Table 2**, the estimated cost of catalyst preparation ranges from USD2.13 to USD20.99 for the biochar-supported catalyst and from USD5.16 to USD27.66 for the commercial catalyst. This analysis demonstrates that the biochar-supported catalyst not only achieves five times the methanol production efficiency but is also more cost-effective, offering a significant economic advantage.

5. Conclusions

The biochar-supported Cu/ZnO catalyst developed in this study exhibited outstanding methanol production under mild conditions, with a yield nearly five times greater than that of the commercially available Cu/ZnO catalyst supported on Al_2O_3. Moreover, it demonstrated superior selectivity and stability compared to the ternary $Cu/ZnO/Al_2O_3$ catalyst. This exceptional performance is attributed to the efficient dispersion and formation of ultrasmall Cu and ZnO nanoparticles, which resulted in a high concentration of Cu-Zn interfacial sites and abundant oxygen vacancies in the biochar-supported catalyst. Additionally, the biochar's role in enhancing the adsorption and activation of reactants was confirmed through in-depth characterization studies.

The biochar-supported catalyst introduced in this work exhibited superior catalytic performance relative to most previously reported catalysts. The use of a waste-derived support suggests that this catalyst holds promise from both an economic and environmental standpoint. However, several key areas warrant further investigation in future studies. Firstly, biochar derived from different biomass sources should be explored as a support for Cu/ZnO nanoparticles to determine if biochar samples with varying physicochemical and structural properties exhibit differing capabilities in immobilizing Cu/ZnO nanoparticles. Additionally, the potential of biochar as a support for other methanol synthesis catalysts, such as $Cu/ZnO/CeO_2$ and $Cu/ZnO/ZrO_2$, should be investigated.

To establish its versatility as a support for different nanocomposites. Furthermore, the investigation of the impurities present in biochar, such as residual metals, etc., and their effect on the catalytic performance of the resulting catalyst could be highly beneficial. In addition, economic and environmental assessments are proposed to be carried out to compare the cost effectiveness and environmental friendliness of the biochar-supported catalyst with those of other materials. Ultimately, conducting a comprehensive life cycle assessment (LCA) is essential to fully evaluate the economic viability and environmental impact of the biochar-supported catalyst developed in this study.

Acknowledgements

This study was financially supported by the Spanish *Ministerio de Ciencia e Innovación* in the call *Proyectos de Transición Ecológica y Transición Digital 2022*. Squeezer project, ref. TED2021-130407B-I00. Authors acknowledge the use of instrumentation financed through Grant IU16-014206 (METCAM-FIB) to ICN2 funded by the European Union through the European Regional Development Fund (ERDF), with the support of the Ministry of Research and Universities, Generalitat de Catalunya.

Table 2.
Materials and energy costs for the preparation of catalysts.

Parameter	Biochar-supported catalyst	$Cu/ZnO/Al_2O_3$
$Cu(NO_3)_2{\cdot}3H_2O$	0.4 g per 500 mg biochar (~USD0.002 to USD0.024)	0.6 g per 1 g catalyst (~USD0.003 to USD0.036)
$Zn(NO_3)_2{\cdot}6H_2O$	0.246 g per 500 mg biochar (~USD0.0005 to USD0.0025)	0.3 g per 1 g catalyst (~USD0.0006 to USD0.003)
Biochar	500 mg per batch (~USD0.01 to USD0.15)	Not used
Al_2O_3	Not used	10 wt.% of catalyst (~USD0.03 to USD0.05)
Na_2CO_3	Negligible	Negligible
Energy Cost for Biochar Treatment	EUR0.09 per kg of biochar processed	Same calcination energy cost for both catalysts (~EUR 0.09)
Energy Cost for Reduction Process	EUR0.06 per kg of catalyst	EUR0.06 per kg of catalyst

Please cite this article as: Vali S.A., Moral-Vico J., Font X., Sánchez A. Biochar-supported highly dispersed ultrasmall Cu/ZnO nanoparticles as a highly efficient novel catalyst for CO_2 hydrogenation to methanol. Biofuel Research Journal 46 (2025) 2398-2411. DOI: 10.18331/BRJ2025.12.2.3.

References

[1] Alexis Parra-Orobio, B., Soto-Paz, J., Ricardo Oviedo-Ocaña, E., Vali, S.A., Sánchez, A., 2023. Advances, trends and challenges in the use of biochar as an improvement strategy in the anaerobic digestion of organic waste: a systematic analysis. Bioengineered. 14(1).

[2] An, B., Zhang, J., Cheng, K., Ji, P., Wang, C., Lin, W., 2017. Confinement of ultrasmall Cu/ZnOx nanoparticles in metal-organic frameworks for selective methanol synthesis from catalytic hydrogenation of CO_2, J. Am. Chem. Soc. 139, 3834-3840.

[3] Araújo, T.P., Mondelli, C., Agrachev, M., Zou, T., Willi, P.O., Engel, K.M., Grass, R.N., Stark, W.J., Safonova, O.V., Jeschke, G., Mitchell, S., 2022. Flame-made ternary Pd-In_2O_3-ZrO_2 catalyst with enhanced oxygen vacancy generation for CO_2 hydrogenation to methanol. Nat. Commun. 13(1), p.5610.

[4] Barlocco, I., Maleki, F., Pacchioni, G., 2023. CO_2 Activation on Cu/TiO_2 nanostructures: importance of dual binding site. Chem-A Europ. J. 29(36), e202300757.

[5] Behrens, M., Studt, F., Kasatkin, I., Kühl, S., Hävecker, M., Abild-Pedersen, F., Zander, S., Girgsdies, F., Kurr, P., Kniep, B.L., Tovar, M., Fischer, R.W., Nørskov, J.K., Schlögl, R., 2012. The Active Site of Methanol Synthesis over Cu/ZnO/Al_2O_3 Industrial Catalysts. Science. 336(6083), 893-897.

[6] Bonura, G., Cordaro, M., Cannilla, C., Arena, F., Frusteri, F., 2014. The changing nature of the active site of Cu-Zn-Zr catalysts for the CO_2 hydrogenation reaction to methanol, Appl. Catal. B. 152-153, 152-161.

[7] Cao, X., Sun, S., Sun, R., 2017. Application of biochar-based catalysts in biomass upgrading: a review. RSC Adv. 7(77), 48793-48805.

[8] Cha, J.S., Park, S.H., Jung, S.C., Ryu, C., Jeon, J.K., Shin, M.C., Park, Y.K., 2016. Production and utilization of biochar: a review. J. Ind. Eng. Chem. 40, 1-15.

[9] Chen, G Chen, G., Yu, J., Li, G., Zheng, X., Mao, H., Mao, D., 2023. Cu+-ZrO_2 interfacial sites with highly dispersed copper nanoparticles derived from Cu@UiO-67 hybrid for efficient CO_2 hydrogenation to methanol. Int. J. Hydrogen Energy. 48(7), 2605-2616.

[10] Ding, J., Jiang, R., Hu, S., Du, B., Li, Y., Wang, Yerong, Qiao, W., Wang, Z., Wang, Yanming, Yu, G., Guo, X., Wang, Yuqing, 2025. Enhanced selectivity to methanol in CO_2 hydrogenation on CuO/ZrO_2 catalysts by alkali metal modification. ChemCatChem. 17(2), e202401400.

[11] Du, S., Tang, W., Lu, X., Wang, S., Guo, Y., Gao, P.X., 2018. Cu-decorated ZnO nanorod array integrated structured catalysts for low-pressure CO_2 hydrogenation to methanol. Adv. Mater. Interfaces. 5(3), 1700730.

[12] Fan, Y.J., Wu, S.F., 2016. A graphene-supported copper-based catalyst for the hydrogenation of carbon dioxide to form methanol. J. CO_2 Util. 16, 150-156.

[13] Fichtl, M.B., Schumann, J., Kasatkin, I., Jacobsen, N., Behrens, M., Schlögl, R., Muhler, M., Hinrichsen, O., 2014. Counting of oxygen defects versus metal surface sites in methanol synthesis catalysts by different probe molecules. Angew. Chemie-Int. Ed. 53(27), 7043-7047.

[14] Fritsch, C., Dornseiffer, J., Blankenstein, J., Noyong, M., Groteklaes, C., Simon, U., 2024. CO_2-Hydrogenation to methanol over CuO/ZnO based infiltration composite catalyst spheres. ChemCatChem. 16(21), e202400731.

[15] Gaikwad, R., Bansode, A., Urakawa, A., 2016. High-pressure advantages in stoichiometric hydrogenation of carbon dioxide to methanol. J. Catal. 343, 127-132.

[16] Gutterød, E.S., Lazzarini, A., Fjermestad, T., Kaur, G., Manzoli, M., Bordiga, S., Svelle, S., Lillerud, K.P., Skúlason, E., Øien-ØDegaard, S., Nova, A., Olsbye, U., 2020. Hydrogenation of CO_2 to methanol by Pt nanoparticles encapsulated in UiO-67: deciphering the role of the metal-organic framework. J. Am. Chem. Soc. 142(2), 999-1009.

[17] Huang, C., Chen, S., Fei, X., Liu, D., Zhang, Y., 2015. Catalytic hydrogenation of CO_2 to methanol: study of synergistic effect on adsorption properties of CO_2 and H_2 in CuO/ZnO/ZrO_2 system. Catalysts. 5(4), 1846-1861.

[18] Jadhav, S.G., Vaidya, P.D., Bhanage, B.M., Joshi, J.B., 2014. Catalytic carbon dioxide hydrogenation to methanol: a review of recent studies. Chem. Eng. Res. Des. 92(11), 2557-2567.

[19] Jain, G., Rocks, C., Maguire, P., Mariotti, D., 2020. One-step synthesis of strongly confined, defect-free and hydroxy-terminated ZnO quantum dots. Nanotechnology. 31.

[20] Kattel, S., Liu, P., Chen, J.G., 2017a. Tuning selectivity of CO_2 hydrogenation reactions at the metal/oxide interface. J. Am. Chem. Soc. 139(29), 9739-9754.

[21] Kattel, S., Ramírez, P.J., Chen, J.G., Rodriguez, J.A., Liu, P., 2017b. Active sites for CO_2 hydrogenation to methanol on Cu/ZnO catalysts. Science. 355(6331), 1296-1299.

[22] Lee, J., Kim, K.H., Kwon, E.E., 2017. Biochar as a catalyst. Renew. Sust. Energy Rev. 77, 70-79.

[23] Lei, H., Nie, R., Wu, G., Hou, Z., 2015. Hydrogenation of CO_2 to CH_3OH over Cu/ZnO catalysts with different ZnO morphology. Fuel. 154, 161-166.

[24] Leung, D.Y.C., Caramanna, G., Maroto-Valer, M.M., 2014. An overview of current status of carbon dioxide capture and storage technologies. Renew. Sust. Energy Rev. 39, 426-443.

[25] Li, B., Wang, F., Li, K., Ning, P., Chen, M., Zhang, C., 2023. CeO_2-supported Fe, Co and Ni toward CO_2 hydrogenation: tuning catalytic performance via metal-support interaction. J. Rare Earth. 41(6), 926-932.

[26] Liao, X., Zhang, Y., Guo, J., Zhao, L., Hill, M., Jiang, Z., Zhao, Y., 2017. The catalytic hydrogenation of maleic anhydride on CeO_2-δ-supported transition metal catalysts. Catalysts. 7(9), 272.

[27] Mahmoud, S.A., Elsisi, M.E., Mansour, A.F., 2022. Synthesis and electrochemical performance of α-Al_2O_3 and M-Al_2O_4 spinel nanocomposites in hybrid quantum dot-sensitized solar cells. Sci. Rep. 12, 17009.

[28] Markewitz, P., Kuckshinrichs, W., Leitner, W., Linssen, J., Zapp, P., Bongartz, R., Schreiber, A., Müller, T.E., 2012. Worldwide innovations in the development of carbon capture technologies and the utilization of CO_2,. Energy Environ. Sci. 5(6), 7281-7305.

[29] Mitsuka, Y., Ogiwara, N., Mukoyoshi, M., Kitagawa, H., Yamamoto, T., Toriyama, T., Matsumura, S., Haneda, M., Kawaguchi, S., Kubota, Y., Kobayashi, H., 2021. Fabrication of integrated copper-based nanoparticles/amorphous metal-organic framework by a facile spray-drying method: highly enhanced CO_2 hydrogenation activity for methanol synthesis. Angew. Chemie-Int. Ed. 60(41), 22283-22288.

[30] Olsbye, U., Nova, A., Gutterød, E.S., Pulumati, S.H., Kaur, G., Lazzarini, A., Solemsli, B.G., Gunnæs, A.E., Ahoba-Sam, C., Kalyva, M.E., Sannes, J.A., Svelle, S., Skúlason, E., 2020. Influence of defects and H_2O on the hydrogenation of CO_2 to methanol over pt nanoparticles in UiO-67 metal-organic framework. J. Am. Chem. Soc. 142(40), 17105-17118.

[31] Palomino, R.M., Ramírez, P.J., Liu, Z., Hamlyn, R., Waluyo, I., Mahapatra, M., Orozco, I., Hunt, A., Simonovis, J.P., Senanayake, S.D., Rodriguez, J.A., 2018. Hydrogenation of CO_2 on ZnO/Cu(100) and ZnO/Cu(111) catalysts: role of copper structure and metal-oxide interface in methanol synthesis. J. Phys. Chem. B. 122(2), 794-800.

[32] Pereira Lopes, R., Astruc, D., 2021. Biochar as a support for nanocatalysts and other reagents: recent advances and applications. Coord. Chem. Rev. 426, 213585.

[33] Phongamwong, T., Chantaprasertporn, U., Witoon, T., Numpilai, T., Poo-arporn, Y., Limphirat, W., Donphai, W., Dittanet, P., Chareonpanich, M., Limtrakul, J., 2017. CO_2 hydrogenation to methanol over CuO-ZnO-ZrO2-SiO_2 catalysts: effects of SiO_2 contents. Chem. Eng. J. 316, 692-703.

[34] Raudaskoski, R., Turpeinen, E., Lenkkeri, R., Pongrácz, E., Keiski, R.L., 2009. Catalytic activation of CO_2: use of secondary CO_2 for the production of synthesis gas and for methanol synthesis over copper-based zirconia-containing catalysts. Catal. Today. 144(3-4), 318-323.

[35] Shi, Z., Tan, Q., Wu, D., 2019. Enhanced CO_2 hydrogenation to methanol over TiO_2 nanotubes-supported CuO-ZnO-CeO_2 catalyst. Appl. Catal. A Gen. 581, 58-66.

[36] Si, C., Ban, H., Chen, K., Wang, X., Cao, R., Yi, Q., Qin, Z., Shi, L., Li, Z., Cai, W., Li, C., 2020. Insight into the positive effect of Cu^0/Cu^+ ratio on the stability of Cu-ZnO-CeO_2 catalyst for syngas hydrogenation. Appl. Catal. A Gen. 594, 117466.

Please cite this article as: Vali S.A., Moral-Vico J., Font X., Sánchez A. Biochar-supported highly dispersed ultrasmall Cu/ZnO nanoparticles as a highly efficient novel catalyst for CO_2 hydrogenation to methanol. Biofuel Research Journal 46 (2025) 2398-2411. DOI: 10.18331/BRJ2025.12.2.3.

[37] Song, X., Yang, C., Li, X., Wang, Z., Pei, C., Zhao, Z.J., Gong, J., 2022. On the role of hydroxyl groups on Cu/Al_2O_3in CO_2 hydrogenation. ACS Catal. 12(22), 14162-14172.
[38] Stawowy, M., Ciesielski, R., Maniecki, T., Matus, K., Łużny, R., Trawczynski, J., Silvestre-Albero, J., Łamacz, A., 2020. CO_2 hydrogenation to methanol over Ce and Zr containing UiO-66 and Cu/UiO-66. Catalysts. 10(1), 39.
[39] Toyir, J., Saito, M., Yamauchi, I., Luo, S., Wu, J., Takahara, I., Takeuchi, M., 1998. Development of high performance Raney Cu-based catalysts for methanol synthesis from CO_2 and H_2. Catal. Today. 45(1-4), 245-250.
[40] Ullah Awan, S., Hasanain, S.K., Bertino, M.F., Hassnain Jaffari, G., 2012. Ferromagnetism in Li doped ZnO nanoparticles: the role of interstitial Li. J. Appl. Phys. 112(10), 103924.
[41] Vali, S.A., Baghdadi, M., Abdoli, M.A., 2018. Immobilization of polyaniline nanoparticles on the polyurethane foam derived from waste materials: a porous reactive fixed-bed medium for removal of mercury from contaminated waters. J. Environ. Chem. Eng. 6(5), 6612-6622.
[42] Vali, S.A., Moral-Vico, J., Font, X., Sánchez, A., 2023a. Adsorptive removal of siloxanes from biogas: recent advances in catalyst reusability and water content effect, Biomass Convers. Biorefin. 14, 23259-23273.
[43] Vali, S.A., Markeb, A.A., Moral-Vico, J., Font, X., Sánchez, A., 2023b. Recent advances in the catalytic conversion of methane to methanol: from the challenges of traditional catalysts to the use of nanomaterials and metal-organic frameworks. Nanomaterials. 13.
[44] Vali, S.A., Markeb, A.A., Moral-Vico, J., Font, X., Sánchez, A., 2023c. A novel Cu-based catalyst supported in chitosan nanoparticles for the hydrogenation of carbon dioxide to methanol: from the optimization of the catalyst performance to the reaction mechanism. Catal. Commun. 182, 106747.
[45] Vali, S.A., Moral-Vico, J., Font, X., Sánchez, A., 2024. $Cu/ZnO/CeO_2$ sSupported on MOF-5 as a novel catalyst for the CO_2 hydrogenation to methanol: a mechanistic study on the effect of CeO_2 and MOF-5 on active sites. Catal. Letters. 154, 3157-3173.
[46] Van Den Berg, R., Prieto, G., Korpershoek, G., Van Der Wal, L.I., Van Bunningen, A.J., Lægsgaard-Jørgensen, S., De Jongh, P.E., De Jong, K.P., 2016. Structure sensitivity of Cu and CuZn catalysts relevant to industrial methanol synthesis. Nat. Commun. 7, 13057.
[47] Wang, Y., 2017. Catalytic hydrogenation of CO_2 to methanol via MOF-confined ultrasmall Cu/ZnOx nanoparticles, Wuli Huaxue Xuebao/ Acta Physico - Chimica Sinica. 33(5), 857-858.
[48] Wesner, A., Kampe, P., Herrmann, N., Eller, S., Ruhmlieb, C., Albert, J., 2023. Indium-based Catalysts for CO_2 Hydrogenation to Methanol: key Aspects for Catalytic Performance. ChemCatChem. 15(24), e202301125.
[49] Xin, Y., Li, Q., Wang, S., Hu, S., Wang, L., 2023. Cu/Nb_2O_5 composite aerogel for CO_2 hydrogenation to methanol: construction of porous structure and abundant active interfaces. Chem. Eng. J. 470, 144289.
[50] Xin, Y., Wang, S., Yuan, H., Hou, T., Zhu, W., Liu, Y., Yao, Y., Zhang, W., Liang, S., Wang, L., 2021. Atomic-level insights into the activation of nitrogen via hydrogen-bond interaction toward nitrogen photofixation. Chem. 7(8), 2118-2136.
[51] Yang, K., Jiang, J., 2020. Computational design of a metal-based frustrated Lewis pair on defective UiO-66 for CO_2 hydrogenation to methanol. J. Mater. Chem. A Mater. 8(43), 22802-22815.
[52] Yang, Y., Xu, Y., Ding, H., Yang, D., Cheng, E., Hao, Y., Wang, H., Hong, Y., Su, Y., Wang, Y., Peng, L., Li, J., 2021. Cu/ZnOx@UiO-66 synthesized from a double solvent method as an efficient catalyst for CO_2 hydrogenation to methanol. Catal. Sci. Technol. 11(13), 4367-4375.
[53] Yu, J., Chen, G., Guo, Q., Guo, X., Da Costa, P., Mao, D., 2022. Ultrasmall bimetallic Cu/ZnOx nanoparticles encapsulated in UiO-66 by deposition-precipitation method for CO_2 hydrogenation to methanol. Fuel. 324(Part B), 124694.
[54] Yu, J., Liu, S., Mu, X., Yang, G., Luo, X., Lester, E., Wu, T., 2021a. Cu-ZrO_2 catalysts with highly dispersed Cu nanoclusters derived from ZrO_2@ HKUST-1 composites for the enhanced CO_2 hydrogenation to methanol. Chem. Eng. J. 419, 129656.
[55] Yu, K., Jiang, P., Yuan, H., He, R., Zhu, W., Wang, L., 2021b. Cu-based nanocrystals on ZnO for uranium photoreduction: plasmon-assisted activity and entropy-driven stability. Appl. Catal., B. 288, 119978.
[56] Zander, S., Seidlhofer, B., Behrens, M., 2012. In situ EDXRD study of the chemistry of aging of co-precipitated mixed Cu, Zn hydroxycarbonates - consequences for the preparation of Cu/ZnO catalysts. Dalton Trans. 41(43), 13413-13422.
[57] Zhang, F., Xu, X., Qiu, Z., Feng, B., Liu, Y., Xing, A., Fan, M., 2022. Improved methanol synthesis performance of $Cu/ZnO/Al_2O_3$ catalyst by controlling its precursor structure. Green Energy Environ. 7(4), 772-781.
[58] Zhang, L.X., Zhang, Y.C., Chen, S.Y., 2011. Effect of promoter TiO_2 on the performance of $CuO-ZnO-Al_2O_3$ catalyst for CO_2 catalytic hydrogenation to methanol. J. Fuel Chem. Technol. 39(12), 912-917.
[59] Zhao, H., Yu, R., Ma, S., Xu, K., Chen, Y., Jiang, K., Fang, Y., Zhu, C., Liu, X., Tang, Y., Wu, L., Wu, Y., Jiang, Q., He, P., Liu, Z., Tan, L., 2022. The role of $Cu1-O_3$ species in single-atom Cu/ZrO_2 catalyst for CO_2 hydrogenation. Nat Catal. 5(9), 818-831.
[60] Zhao, Y.F., Yang, Y., Mims, C., Peden, C.H.F., Li, J., Mei, D., 2011. Insight into methanol synthesis from CO_2 hydrogenation on Cu(1 1 1): complex reaction network and the effects of H_2O. J. Catal. 281, 199-211.

Seyed Alireza Vali is a Ph.D. researcher at Universitat Autonoma de Barcelona (UAB), Spain. He has a Master's degree in Environmental engineering from University of Tehran, Iran, and a Bachelor`s Degree in Civil engineering from Shahid Beheshti University, Iran. He has previously published over 7 peer-reviewed journal papers covering a wide range of subjects within environmental chemical engineering and catalysis. His research interests include (1) biogas upgrading technologies; (2) nanomaterials; (3) catalysis; and (4) water treatment. His research profile on Google Scholar can be found at the following link: https://scholar.google.com/citations?user=7ipLO1oAAAAJ&hl=en

Javier Moral-Vico is an associate professor in the Department of Chemical, Biological and Environmental Engineering of Universitat Autònoma de Barcelona (UAB), Spain. He obtained his Master Degree in Nanomaterials at the University of Pavia (Italy), and his Ph. D. in Materials Science at the Materials Science Institute of Barcelona (ICMAB-CSIC). He is currently working in the applications of nanomaterials in environmental engineering, and has several publications in topics such as of GHGs catalysis, water pollutants remediation and the use of nanomaterials in anaerobic digestion.

Please cite this article as: Vali S.A., Moral-Vico J., Font X., Sánchez A. Biochar-supported highly dispersed ultrasmall Cu/ZnO nanoparticles as a highly efficient novel catalyst for CO_2 hydrogenation to methanol. Biofuel Research Journal 46 (2025) 2398-2411. DOI: 10.18331/BRJ2025.12.2.3.

Dr. Xavier Font is a Full Professor in the Department of Chemical, Biological, and Environmental Engineering at Universitat Autònoma de Barcelona, Spain. He is a chemist and holds a PhD in Science. His research focuses on two main areas: the valorization of organic solid waste (anaerobic digestion, composting, and solid-state fermentation) and the use of nanomaterials for environmental applications (enhancing anaerobic digestion, adsorption, and using nanomaterials as catalysts).

Dr. Antoni Sánchez leads the Composting Research Group (https://webs.uab.cat/gicom/en/) since year 2000. He works as full professor in the Department of Chemical, Biological and Environmental Engineering of Autonomous University of Barcelona. His research lines cover the main aspects involved in the treatment of organic solid waste, through several strategies. Composting, anaerobic digestion for biogas production and solid-state fermentation are the main lines. He has participated and coordinated several Spanish and European projects on this topic, supervised PhD and Master Thesis and is the author of more than 200 indexed papers as well as book chapters and patents. His research profile on Google Scholar can be found at the following link:
https://scholar.google.com/citations?user=f2hh0z8AAAAJ&hl=ca

Please cite this article as: Vali S.A., Moral-Vico J., Font X., Sánchez A. Biochar-supported highly dispersed ultrasmall Cu/ZnO nanoparticles as a highly efficient novel catalyst for CO_2 hydrogenation to methanol. Biofuel Research Journal 46 (2025) 2398-2411. DOI: 10.18331/BRJ2025.12.2.3.

Supplementary Information

Table S1.
The chemical amounts used for the synthesis of samples.

Sample	Biochar (mg)	$Cu(NO_3)_2 \cdot 3H_2O$ (mmol)	$Zn(NO_3)_2 \cdot 6H_2O$ (mmol)	$Al(NO_3)_3.9H_2O$
1-20%Cu/ZnO@BC	500	0.827	0.827	/
1-25%Cu/ZnO@BC	500	1.240	1.240	/
1-29%Cu/ZnO@BC	500	1.655	1.655	/
1-37%Cu/ZnO@BC	500	2.482	2.482	/
1-44%Cu/ZnO@BC	500	3.31	3.31	/
1-51%Cu/ZnO@BC	500	4.137	4.137	/
0.5-25%Cu/ZnO@BC	500	0.828	1.655	/
1.5-25%Cu/ZnO@BC	500	1.49	0.993	/
2-25%Cu/ZnO@BC	500	1.655	0.828	/
3-25%Cu/ZnO@BC	500	1.862	0.62	/
4-25%Cu/ZnO@BC	500	1.985	0.496	/
$Cu/ZnO/Al_2O_3$	/	6	3	1
27%Cu@BC	500	2.483	/	/

Table S2.
The elemental composition of the pristine biochar.

Element	Ratio
C %	77.4
H %	2.41
N %	0.7
S %	<0.1
Mg (mg kg^{-1})	1729
Al (mg kg^{-1})	1121
Si (mg kg^{-1})	3140
P (mg kg^{-1})	874
K (mg kg^{-1})	6048
Ca (mg kg^{-1})	18436
Mn (mg kg^{-1})	1785
Fe (mg kg^{-1})	1300
Cu (mg kg^{-1})	10
Zn (mg kg^{-1})	134

Table S3.
Mass ratio of the elements in catalyst samples obtained by inductively coupled plasma optical emission spectroscopy (ICP-OES).

Sample	Mass Ratio of Cu (wt.%)	Mass Ratio of Zn (wt.%)	Mass Ratio of Al (wt.%)
1-20%Cu/ZnO@BC	10.05	9.77	/
1-25%Cu/ZnO@BC	11.50	11.87	/
1-29%Cu/ZnO@BC	14.62	14.26	/
1-37%Cu/ZnO@BC	18.60	18.29	/
1-44%Cu/ZnO@BC	22.55	21.48	/
1-51%Cu/ZnO@BC	25.67	25.55	/
0.5-25%Cu/ZnO@BC	8.49	15.88	/
1.5-25%Cu/ZnO@BC	15.00	8.64	/
2-25%Cu/ZnO@BC	18.00	8.19	/
3-25%Cu/ZnO@BC	19.30	6.20	/
4-25%Cu/ZnO@BC	21.16	5.34	/
$Cu/ZnO/Al_2O_3$	48.59	23.39	3.05
27%Cu@BC	26.46	0.41	/

Table S4.
Porosity results of the catalyst samples.

Sample	BET surface area (m^2/g)	Pore volume (cm^3/g)
Pristine biochar	8	0.012
Thermally treated biochar	51	0.047
2-25%Cu/ZnO@BC	25.52	0.023

Please cite this article as: Vali S.A., Moral-Vico J., Font X., Sánchez A. Biochar-supported highly dispersed ultrasmall Cu/ZnO nanoparticles as a highly efficient novel catalyst for CO_2 hydrogenation to methanol. Biofuel Research Journal 46 (2025) 2398-2411. DOI: 10.18331/BRJ2025.12.2.3.

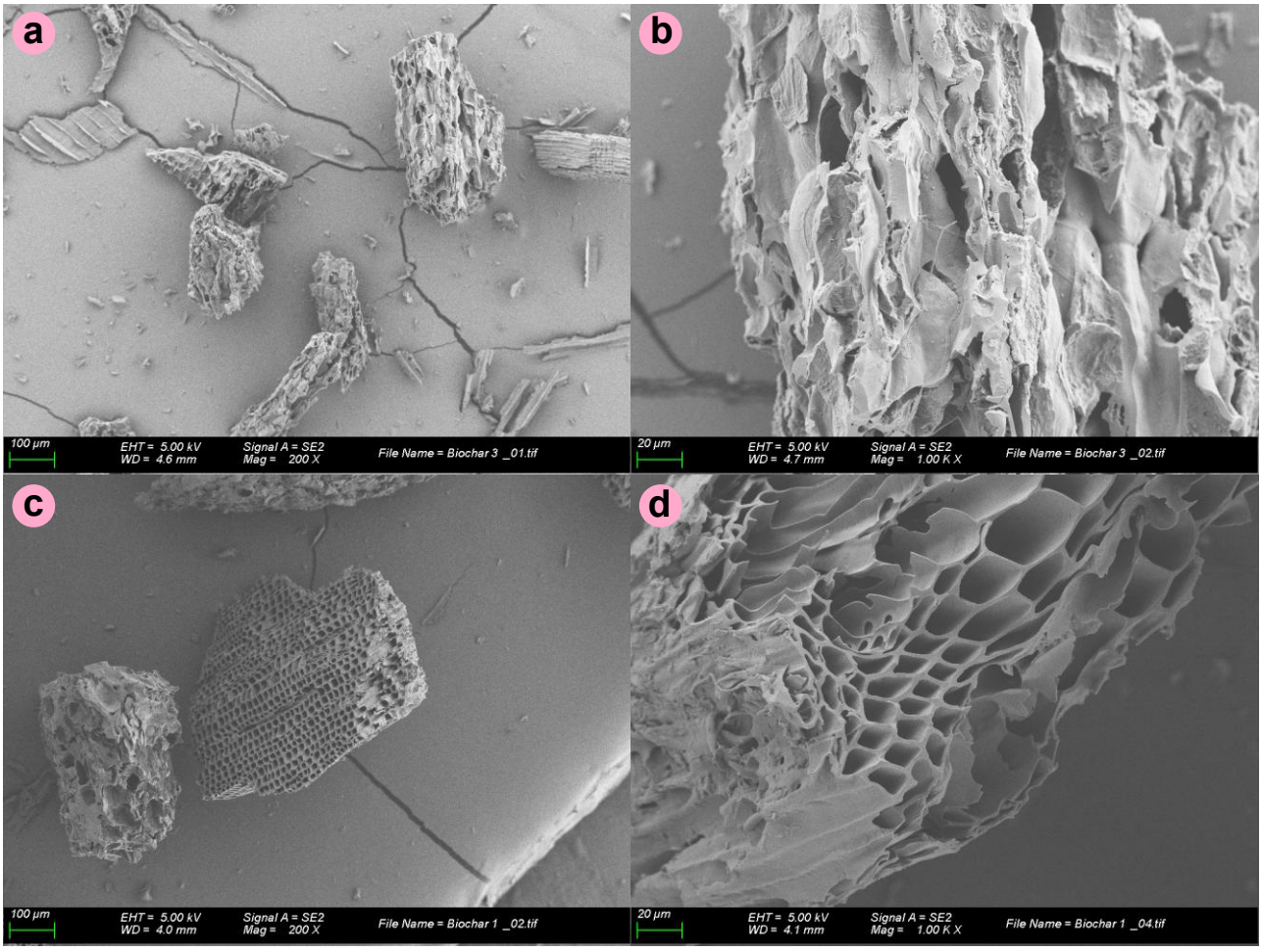

Fig. S1. Scanning electron microscopy images of pristine biochar for two different randomly selected spots in two different scales.

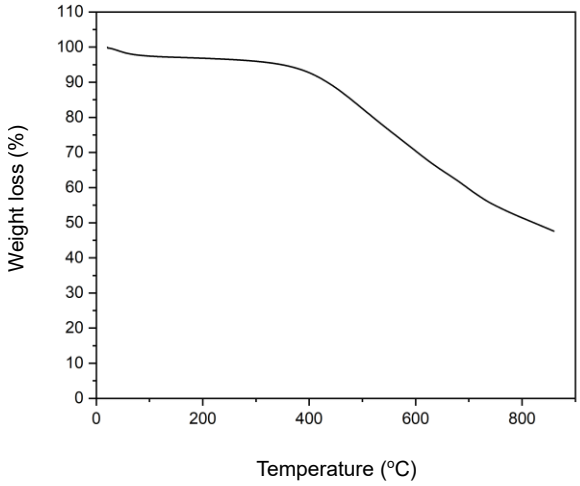

Fig. S2. Thermogravimetry analysis result for used biochar.

Please cite this article as: Vali S.A., Moral-Vico J., Font X., Sánchez A. Biochar-supported highly dispersed ultrasmall Cu/ZnO nanoparticles as a highly efficient novel catalyst for CO_2 hydrogenation to methanol. Biofuel Research Journal 46 (2025) 2398-2411. DOI: 10.18331/BRJ2025.12.2.3.

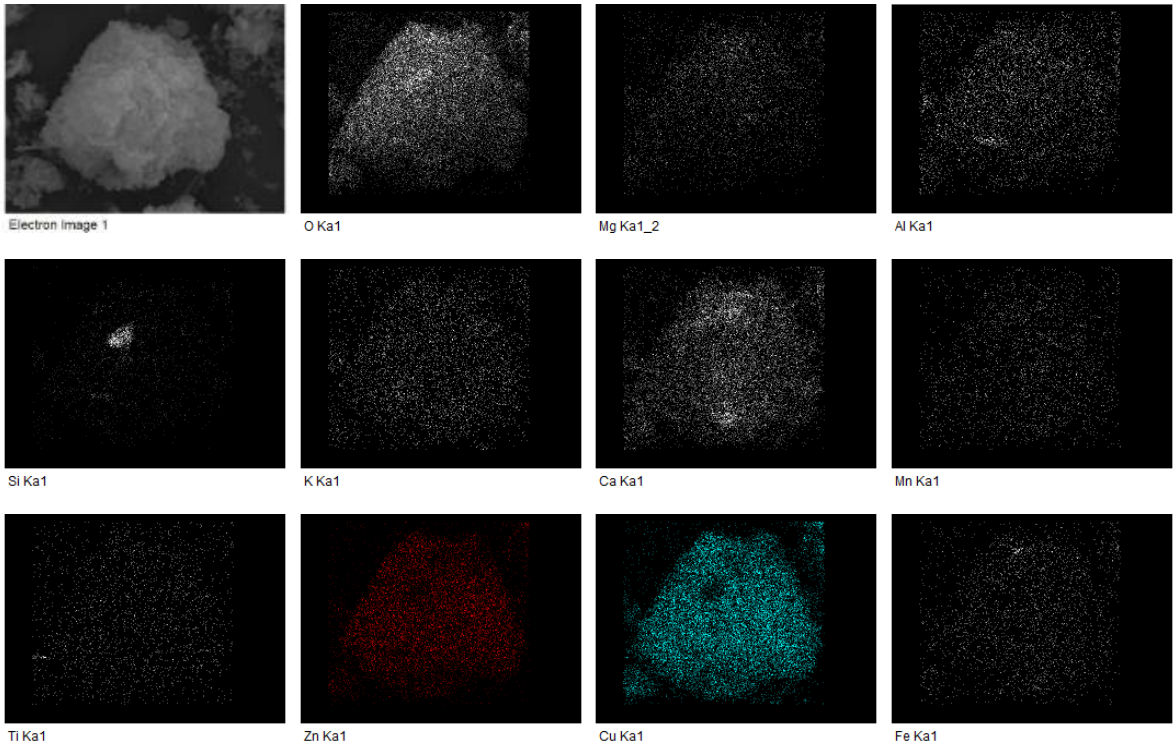

Fig. S3. Energy dispersive spectroscopy (EDX) elemental mapping obtained for the catalyst 2-25%Cu/ZnO@BC.

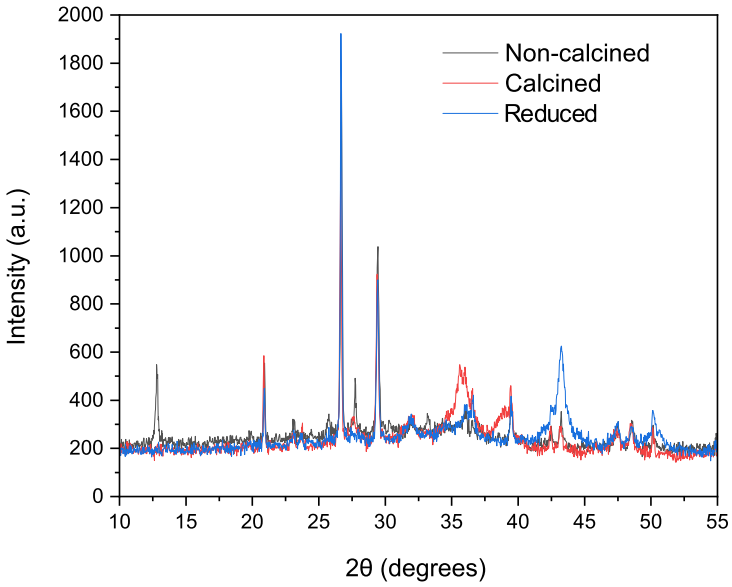

Fig. S4. X-ray diffraction (XRD) patterns for the sample 2-25%Cu/ZnO@BC before calcination, after calcination, and after reduction process.

Please cite this article as: Vali S.A., Moral-Vico J., Font X., Sánchez A. Biochar-supported highly dispersed ultrasmall Cu/ZnO nanoparticles as a highly efficient novel catalyst for CO_2 hydrogenation to methanol. Biofuel Research Journal 46 (2025) 2398-2411. DOI: 10.18331/BRJ2025.12.2.3.

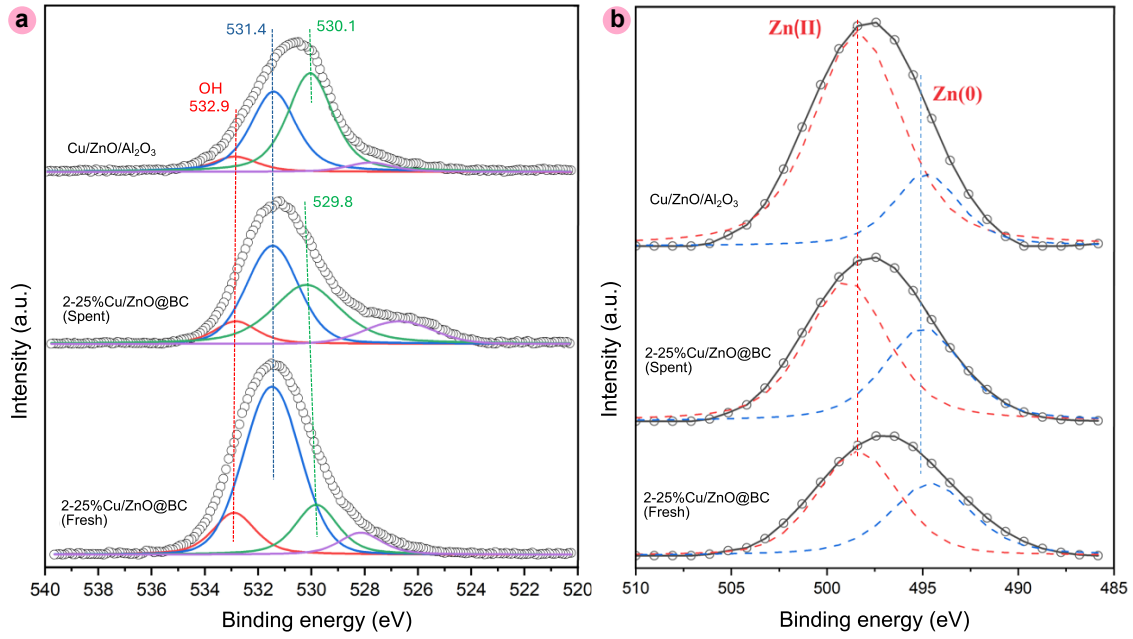

Fig. S5. (a) O 1s, and **(b)** Zn $L_3M_{4.5}M_{4.5}$ Auger X-ray photoelectron spectroscopy (XPS) spectra of 2-25%Cu/ZnO@BC (fresh), 2-25%Cu/ZnO@BC (spent), and Cu/ZnO/Al_2O_3 samples.

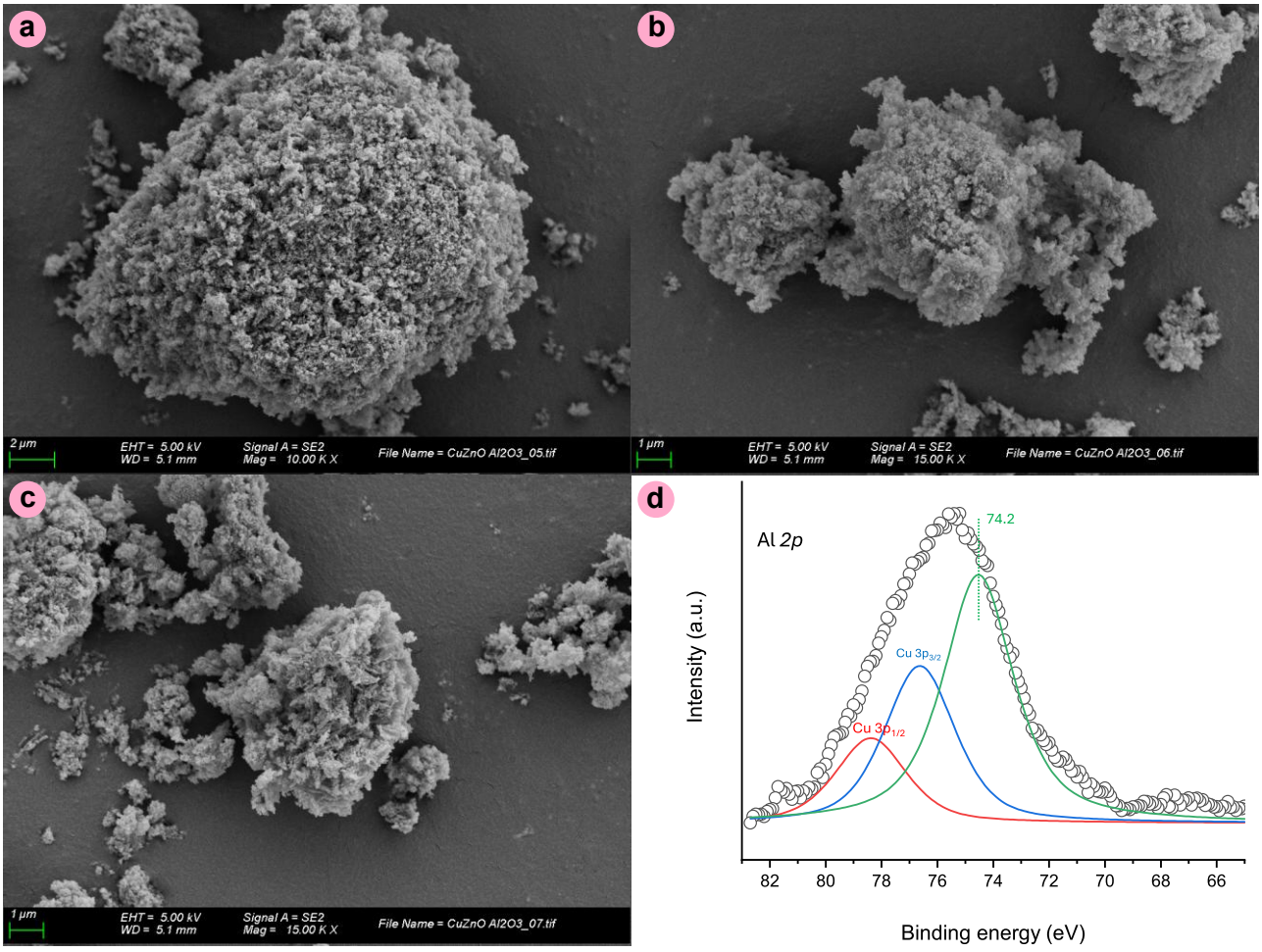

Fig. S6. (a-c) Scanning electron microscopy images and **(d)** Al 2p X-ray photoelectron spectroscopy (XPS) spectra of Cu/ZnO/Al_2O_3 as-synthesized sample.

Please cite this article as: Vali S.A., Moral-Vico J., Font X., Sánchez A. Biochar-supported highly dispersed ultrasmall Cu/ZnO nanoparticles as a highly efficient novel catalyst for CO_2 hydrogenation to methanol. Biofuel Research Journal 46 (2025) 2398-2411. DOI: 10.18331/BRJ2025.12.2.3.

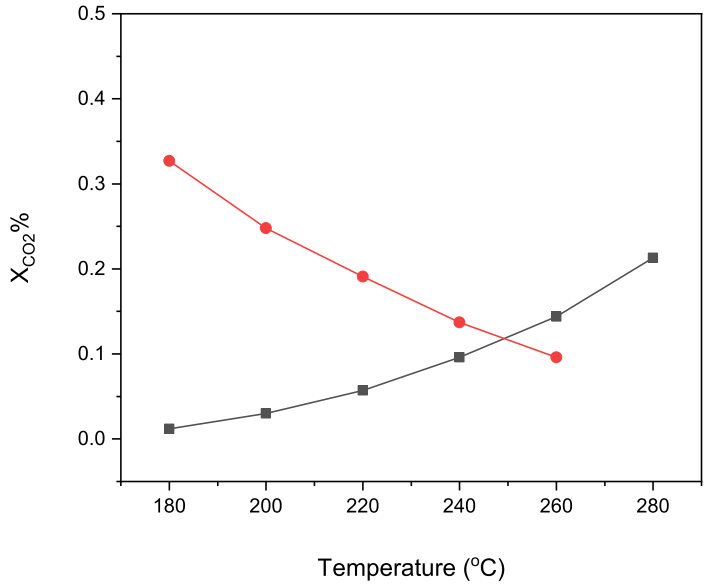

Fig. S7. CO_2 conversion rates over 2-25%-Cu/ZnO@BC under different temperatures (180-280 °C, 1MPa, and 60000 mL·$g_{cat.}^{-1}$·h^{-1}), and different work hourly space velocity (WHSV) (12000-60000 mL·$g_{cat.}^{-1}$·h^{-1}, 240 °C, and 1MPa).

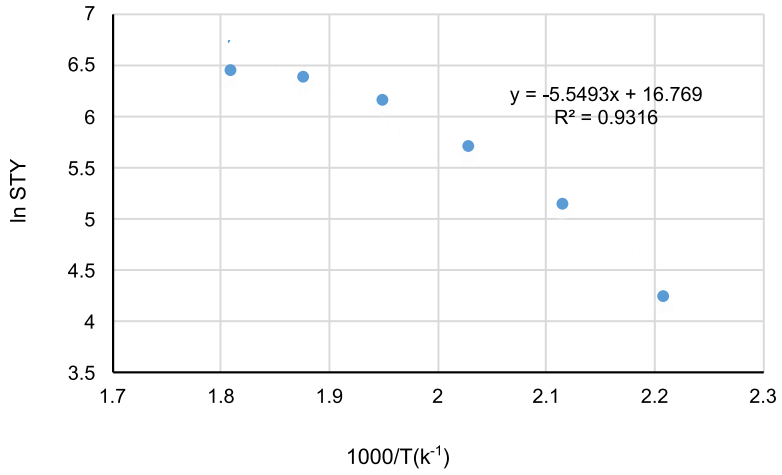

Fig. S8. The Arrhenius plot for methanol synthesis over 2-25%Cu/ZnO@BC.

Please cite this article as: Vali S.A., Moral-Vico J., Font X., Sánchez A. Biochar-supported highly dispersed ultrasmall Cu/ZnO nanoparticles as a highly efficient novel catalyst for CO_2 hydrogenation to methanol. Biofuel Research Journal 46 (2025) 2398-2411. DOI: 10.18331/BRJ2025.12.2.3.

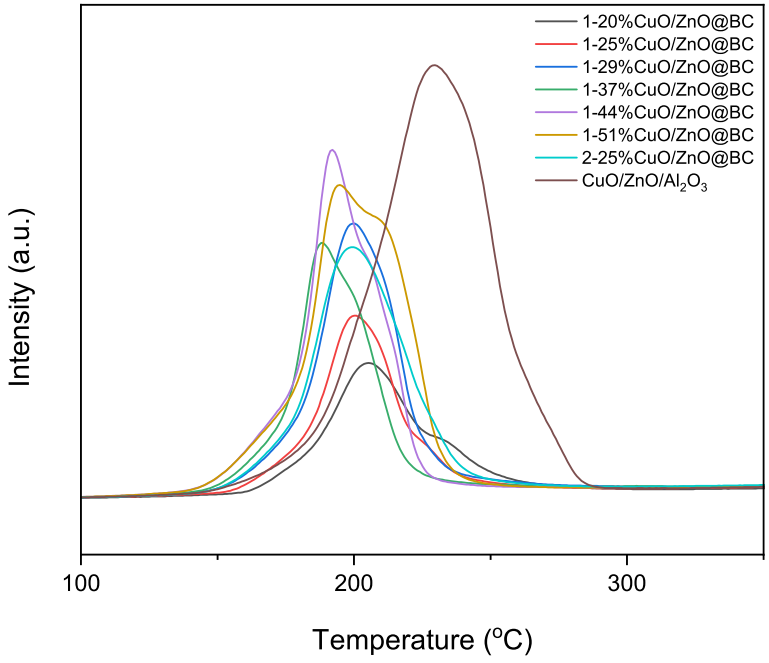

Fig. S9. Hydrogen temperature-programed reduction (H2-TPR) profiles for catalyst samples.

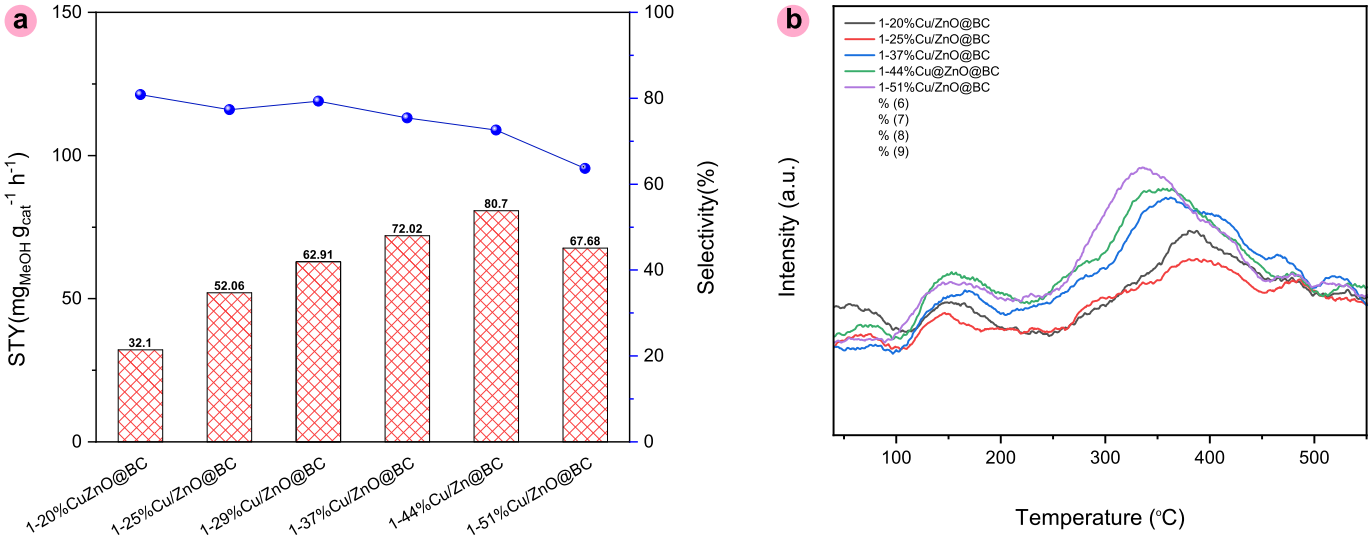

Fig. S10. (a) Methanol Space-time yield (STY) (mg_{MeOH} g_{cat}^{-1} h^{-1}) and **(b)** Hydrogen temperature-programed desorption (H_2-TPD) patterns for the catalyst samples with different contents of NPs.

Please cite this article as: Vali S.A., Moral-Vico J., Font X., Sánchez A. Biochar-supported highly dispersed ultrasmall Cu/ZnO nanoparticles as a highly efficient novel catalyst for CO_2 hydrogenation to methanol. Biofuel Research Journal 46 (2025) 2398-2411. DOI: 10.18331/BRJ2025.12.2.3.